Computational Modeling of coronary blood flow in 3D: An insight into the mechanical environment of atherosclerosis; using Image based FE – Modeling and Fluid Structure Interaction (FSI).

Author

NABISHA FAROOQ

Registration Number

00000170769

Supervisor

Dr. ZARTASHA MUSTANSAR

RESEARCH CENTER FOR MODELING AND SIMULATION

NATIONAL UNIVERSITY OF SCIENCES AND TECHNOLOGY

ISLAMABAD

OCTOBER, 2018

Computational Modeling of coronary blood flow in 3D: An insight into the mechanical environment of atherosclerosis; using Image based FE – Modeling and Fluid Structure Interaction (FSI).

Author
NABISHA FAROOQ
Registration Number
170769

Thesis Supervisor
Dr. ZARTASHA MUSTANSAR

DEPARTMENT OF COMPUTATIONAL ENGINEERING
RESEARCH CENTER FOR MODELING AND SIMULATION
NATIONAL UNIVERSITY OF SCIENCES AND TECHNOLOGY,
ISLAMABAD
OCTOBER, 2018

Thesis Acceptance Certificate

Approval Page

Certificate of Originality

Acknowledgements

Contents

List of Tables

List of Figures

Abstract

Coronary heart disease (CHD) is characterized by the narrowing of coronary arteries and is one of the leading causes of death in today's century. The main cause of CHD is atherosclerosis jots down to the deposition of fat, cholesterol, calcium, and other deposits (collectively called plaque) along the inner lining of the vessel wall. Plaque material and structural characteristics are important factors in the natural progression of the disease and has an important clinical predictive value. Extensive calcification most likely represents a later stage of atherosclerosis and is not only an independent predictor of CHD, but also has prognostic significance in patients with known CHD. The social and economic burden of this disease remains very high. It is important to understand the cause and consequences of CHD.

The main objective of this study is to investigate the role of *hemodynamically induced biomechanical forces* in predicting the mechanical strength of stage v atherosclerotic coronary artery. The uniqueness of this study is coupling of two different techniques (Struture Mechanics and FSI) to investigate plaque burdened coronary vessels.

Author has utilized numerical methods and techniques in computational mechanics and Biomedical Engineering to investigate the synergy of CHD. Three-dimensional image based models of normal and atherosclerotic vessel were built using image processing and a computer solvers. These models were then utilized for the quantification of structural forces induced by the underlying blood flow in a virtual reality set up using Finite Element Modeling. In addition, FSI coupling approach was also employed to address blood-vessel-plaque-simulation. Calcium score was calculated using an algorithm to evaluate its contribution in overall plaque burden. The results obtained validated and compared with the previous literature.

Our results show an increased stiffness and Wall Shear Stress (WSS) in atherosclerotic arteries compared to the healthy ones. Large curvatures under torsional loading are found to be the regions where maximum stress is accumulated making them more vulnerable to the plaque formation &lesions in normal arteries. Moreover, larger strain rates were recorded in healthy arteries and fibrous plaque was found to exhibit stiffest response to loading than calcified lesions. Coronary Artery Calcium Score (CACS) yielded a positive correlation with atherosclerosis and pose a moderate risk of suffering an acute CHD event in the near future.

Briefly, the results obtained from this study are quite promising and poses new avenues as a tool for diagnosis, prevention and better treatment of atherosclerosis. The study may also provide a niche to explore the rare behavior of coronary artery at macro scale.

Key Words: *Coronary heart disease (CHD), Digital Volume Correlation (DVC), Coronary Artery Calcium Score (CACS), Wall Shear Stress (WSS), FSI*

CHAPTER 1: INTRODUCTION

Atherosclerosis is a process of progressive thickening and hardening of arterial walls due to the deposition of fatty components called plaque. Coronary arteries that supplies oxygen rich blood to the heart muscles are among the most susceptible blood vessels. Deposition of these plaque deposits in coronary arteries leads to the coronary heart disease (CHD).

According to the stats published in American Heart Association (2018), CHD ranks first(43.8 %) among the leading cause of death. This research and Investigation into the mechanism of atherosclerosis can be used as a guide in clinical trials.

Various imaging modalities such as CT, MRI and OCT are generally used for the diagnosis of atherosclerosis. Finite elements analysis being one of the popular numerical method has been widely used in the past to address these problem of atherosclerosis.FSI is a popular coupling approach used to address such problems because of its ability to give solution in both fluid and structure domain(Leach et al., 2010, Tang et al., 2004, Costopoulos et al., 2017).

2.1 Research Question

Mapping Progressive damage using image based FE and FSI in atherosclerotic plaques due to hemodynamically induced structural stresses for early prognosis of wall rupture.

2.2 Objectives of the study

- Reconstruction of computationally inexpensive Healthy and Diseased coronary artery models.
- Identification of vulnerable regions in Healthy model prone to plaque formation.
- Compute progressive damage in atherosclerotic plaques for early prognosis of wall rupture.
- Automatic Coronary Artery Calcification (CAC) Scoring.

2.3 Motivation

Heart disease is the leading cause of death for both men and women around the world and Coronary heart disease (CHD) is the most common type of heart disease, killing over 370,000 people annually (CDC, 2015) . In Pakistan, 30 to 40 per cent of all deaths are due

to cardiovascular diseases (Dawn, 2017). My motivation behind the selection of this topic is alarming situation and heritable nature of CHD in Pakistani family. The study will provide insights into the mechanics of CHD using state-of-the-art numerical and computer techniques.

Biomechanical analysis of atherosclerotic plaques is among the top future trends of biomedical engineering. It is one of the areas of research interest among the biomedical community in international conferences. I am personally motivated to look forward for more understanding into mechanics of CHD, so that it is possible to contribute to the knowledge of the field especially in the developing countries like Pakistan. Additionally, there is less evidences in national researches about the mechanical behavior of CHD when coupled with FSI. This study will therefore prove useful for clinical community and medicine, to encourage non-invasive ways of disease treatment and insight for better clinical procedures. .

Furthermore, because the development of Bio-inspired Computational mechanics in Pakistan is still a long way to go, lack of research is being carried out in Pakistan in medical simulation domain. All these factors brought me to choose this topic for the research.

1.4 Relevance to National Needs and Areas of Application

A 3D printed model of atherosclerotic artery based on the image based computational model used in this study can be built and the information gained from the results of this study may allow doctors to create custom fitted stents.

The results of this study are applicable in

- **Healthcare industry:** For the design and evaluation of stents.
- **Medicine:** May help doctors to improve surgical planning in patients with coronary heart disease.
- **Research:** Enable researchers especially biomechanists to have knowledge of the *plaque* strength *that is* crucial for *plaque* rupture prediction.

CHAPTER 2: Literature Review

This chapter covers a review of literature relevant to the study. The chapter has divided into five major sections. First 'anatomy and physiology' of cardiovascular system highlighting the framework of blood vessel is presented. Then developmental stages of atherosclerotic plaque are discussed based on American Heart Association (AHA) classification along with the methods used in some recent studies to investigate atherosclerosis. Various important attributes and approaches use to address fluid structure interaction are also covered to understand the mechanism of interaction in Finite Element suit. Significance of Calcium Scoring in risk stratification of atherosclerotic is enlightened. Finally, the chapter closes with explicating the role of Mechanics in Vasculature.

2.1 Anatomy and Physiology of Cardiovascular System

The heart is a hollow, muscular organ and it is believed to be about the size of one's clenched fist. Anatomically it is located under the sternum and ribcage, and between the two lungs. The heart beats for about 3 billion times in an average life span of a person. The primary function of the heart is to transport blood through the arteries, capillaries, and veins by repeated, rhythmic contractions. These rhythmic contractions occur spontaneously and are governed by muscles of the heart referred as 'cardiac muscles'. These muscles are the main components of the tissues that forms wall of the heart. Unlike skeletal muscles, cardiac muscles are self exciting and don't require any nerve stimulation for activation. Skeletal muscles in contrast become active in response to a conscious stimulus (Moini, 2013).

Heart has four chambers, two upper thin walled atria (singular: atrium) and two lowered thick walled ventricles (figure 2.1). Blood is supplied in right atrium via superior and inferior vena cava. This so called venous blood is poorly oxygenated because it has reached here after circulating the whole body except lungs. Right atrium contracts and pumps the blood into right ventricle which contracts and pushes the blood towards pulmonary arteries that carries it to lungs where the process of respiration takes place and this oxygen depleted blood becomes oxygenated. The blood enters back into the left atrium via pulmonary vein which then contract and pushes this oxygenated blood towards left ventricle from where it is send to whole body.

Because left ventricle's job is to supply blood to whole body it has strong walls thereby generated the misconception that heart lies on the left side(Contributors, 2012).

Septum is the dividing wall between two chambers and in heart two septum are found .One separating two upper atria is called 'inter atrial' septum and second is found between two ventricles referred as 'inter ventricle' septum .

Heart consist of four valves one for each chamber. Aortic and mitral are two atrioventricular (AV) valves present between the atria and ventricles. These are one-way and ensure blood flow from atria to the ventricles, whereas pulmonary and tricuspid valves control the flow of blood out of the ventricles. Lub- dub sound of heart beat is due to the alternate closing of these valves (Moini, 2013).

Each time our heart beats blood enters and leaves the heart in a smooth manner. First aortic and mitral valve opens to fill the atria with blood. When atria contract both aortic and mitral valve shut while pulmonary and tricuspid valves open that pushes he blood out of heart.

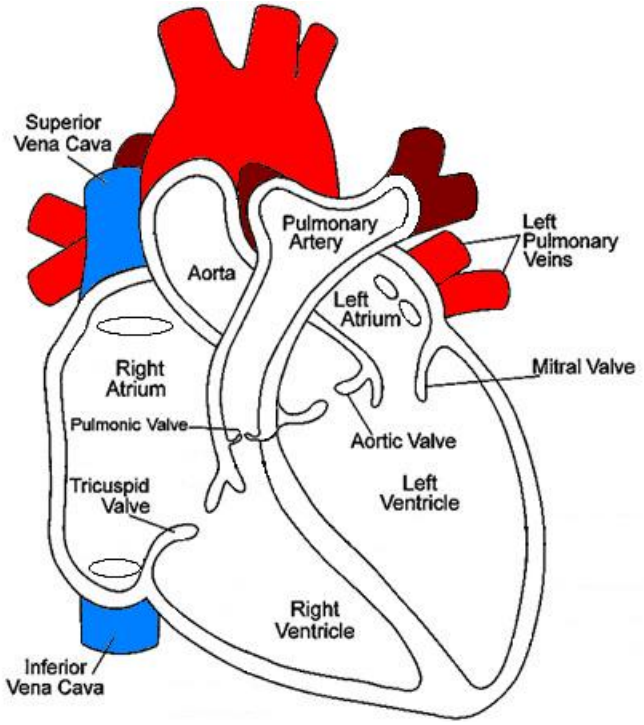

Figure 2.1:HEART'S ANATOMY (cardiac cathpro,2009)

2.1.1 Structural Layers of Heart

Heart is composed of three layers termed as epicardium, myocardium and endocardium (figure 2.2).

- **Epicardium:** The pericardium is the outermost thin layer of serous membrane of heart that protects and provides cushioning to the heart against excessive distension of its muscles. It further consists of two layers an external parietal layer which is made up of connective tissues and inner epicardium separated by a narrow cavity.
- **Myocardium:** The myocardium is middle layer of the heart wall composed of cardiac muscle tissues. It is thick muscular layer responsible for pumping blood thereby generating the need of continuous oxygen and nutrients supply to work efficienly.Mayocardium present beneath epicardium connects it with inner endocardium.
- **Endocardium:** The endocardium is the innermost layer of tissue that lines the chambers of the heart and valves. It is continuous with the endothelial lining of the large blood vessels attached to the heart. The primary role of endocardium is to control the function of mayocardium.It also prevents the formation of blood clots inside heart (Contributors, 2012).

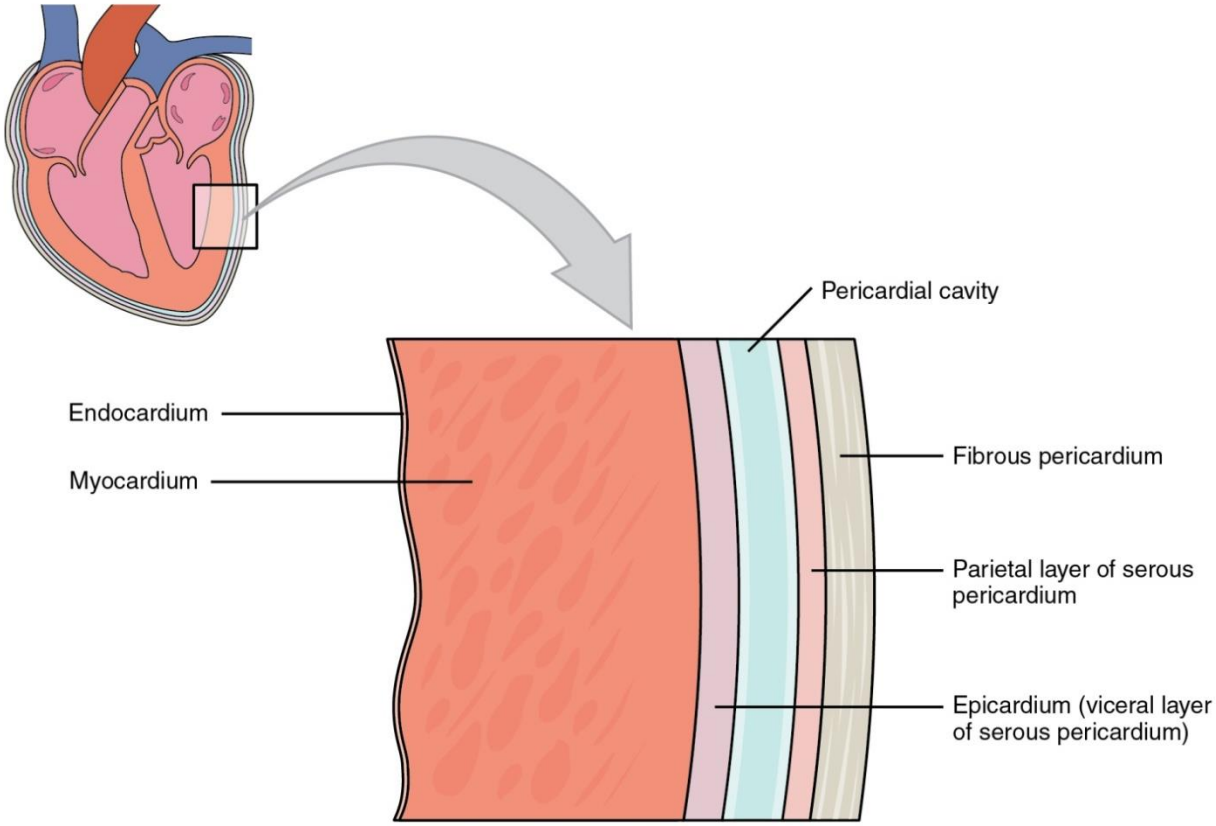

Figure 2.2: Layers of the Heart (Innermost Layer of the Heart, 2018)

2.1.2 Blood Vessels

The three major types of blood vessels found in the human body are artery, veins and capillaries. Role of these blood vessels is to carry blood to every type of tissue and organ. Vessels decrease in size as they move away from the heart. Aorta is the largest artery found in the body whereas vena cava is the largest vein. Blood in the cardiovascular system travels from arteries to veins.

Arteries are elastic vessels that are strong, flexible, and resilient. Their function is to carry blood away from the heart under high pressure. The arteries branch into smaller and smaller vessels, eventually becoming very small vessels called arterioles. Arteries and arterioles have muscular walls that can adjust their diameter through dilation and contraction to increase or decrease blood flows to a particular organ of body .Capillaries are tiny, extremely thin-walled vessels that act as a bridge between arteries and veins. The thin wall of the capillaries allows exchange of nutrients from the blood into tissues and waste products to pass from tissues into the blood. These

capillaries deliver the blood into very small veins called venules, which in turn pass it onto the veins leading to the heart. Veins have much thinner walls than arteries, because of the lower pressure in them (Moini, 2013).

2.1.3 Layers of blood vessels

Blood vessels are usually composed of three layers: the tunica intima, tunica media, and tunica adventitia (figure 2.3). The tunica intima is the innermost lining of blood vessels and consists of a layer of endothelial cells and loose connective tissues. Internal elastic lamina is a thin layer which separates tunica intima from tunica media.

The tunica media is localized between tunica intima and tunica adventitia and is composed of circumferentially arranged smooth muscle cells. In small arteries the arrangement of their muscle fibers is in rough spiral layers.

Finally, tunica adventitia also called as tunica externa is the outermost layer of a blood vessel primarily composed of loose connective tissue made up of fibroblasts and associated collagen fibers.

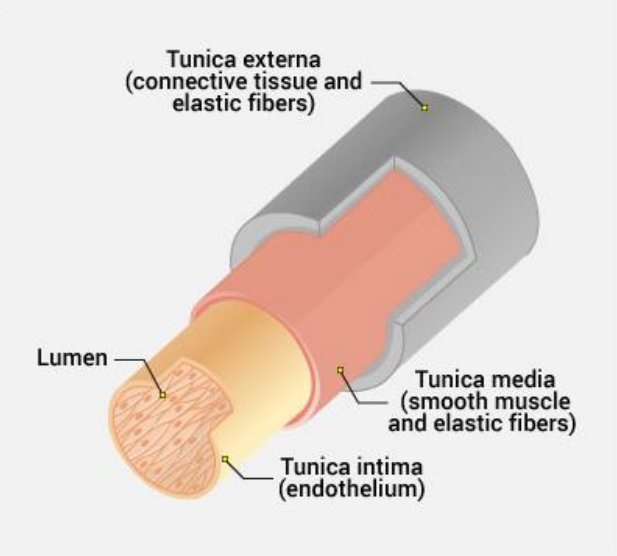

Figure 2.3: Layers of Artery (Blood vessels,2018)

2.1.4 Coronary Arteries

The heart receives its own supply of blood from a set of the coronary arteries. Two major coronary arteries called “Left main coronary artery (LMA)” and **“**Right coronary artery (RCA)” branch off from the aorta (figure 2.4). These arteries and their branches supply blood to all parts of the heart. LMA further branches into **“**Circumflex artery” and “Left Anterior Descending artery (LAD)” whereas RCA further divides into “Right marginal artery (RMA)” and “Posterior descending artery (PDA)”.Research shows that LAD and RCA are more *susceptible to the development of atherosclerotic* lesions (Wasilewski et al., 2015). In this thesis only proximal portion of RCA right before the start of PDA is being analyzed for atherosclerosis risk stratification.

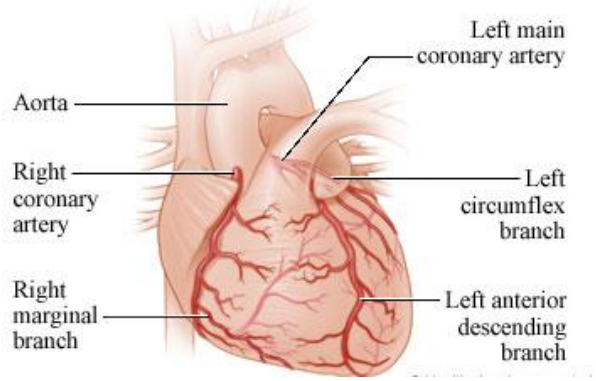

Figure 2.4: Coronary Arteries

2.2 Atherosclerosis

Atherosclerosis refers to the stiffness of the vessels due to the overtime accumulation of the fatty constituents called plaque. It starts with the initial thickening of subintima and leads to the rupture of adventitia ultimately destabilizing its structure. Risk factors of atherosclerosis include Hypertension, Diabetes, obesity, sedentary life style, and genetics (Vogel, 1997).Medical image analysis plays a key role in detecting and diagnosing intra vascular plaques. Management plan includes physical exercises followed by a low calorie diet along with medications such as anti platelets and anti atherogenic (S Antonopoulos et al., 2012).

2.2.1 Classifications of Atherosclerosis

In order to quantify plaque vulnerability, it is necessary to be aware of with the classification of plaque components.AHA has divided these plaque into six categories. Type I, II, and III are non fatal types of lesions while types IV, V, and VI have the potential to be lethal.

Type I is classified as the initial lesion. Although thickening of intima is a natural process starts from birth (Stary et al, 1995) but migration of a large number of macrophages and foam cells marked as stage 1 of atherosclerosis. Type II lesions are characterized by accumulation of lipid to form fatty streaks. Type III is non lethal because till that stage there is no damage to endothelial layer and since size of lipid pool is not big enough so no threat to life was imposed. Type IV is called atheroma lesion and is accompanied by the development of extracellular lipid core.This category is basically an extension of type 3 with large lipid core. Degree to which this lipid core has protruded into the lumen determines the seriousness of condition. Continuous growth of lipid pool can cause severe lumen obstruction and hence can cause the eventuality of stroke (figure 2.5) .It is to be noted that fibrotic tissue is not widespread till this stages.

However in stage 5 extensive fibrous tissue layers are present (hence named fibroatheroma) and can be accompanied with calcium or no lipid pool. In comparison with stage 4, occlusion in stage 5 block the blood flow gradually leading to serious complications. The patient specific dataset used in this study belongs to this category and have calcified and fibrous plaque components in it Type 6 lesions are characterized by fissure, hematoma, and thrombus. Tear in the plaque lesion may cause thrombosis and can cause serious threat to the stability of artery by weaken its structure (“UNDERSTANDING THE THREE MAIN STAGES OF PLAQUE GROWT”,2012) .In arterial sclerosis sequential distortion takes place (from inner intima to outer advential coat).serious complications are result of rupture of unstable plaque components. Four primary regions in the body which are more prone to the formation of plaque are coronary arteries, carotid arteries of brain, renal arteries, and femoral arteries(DeBakey et al., 1985).

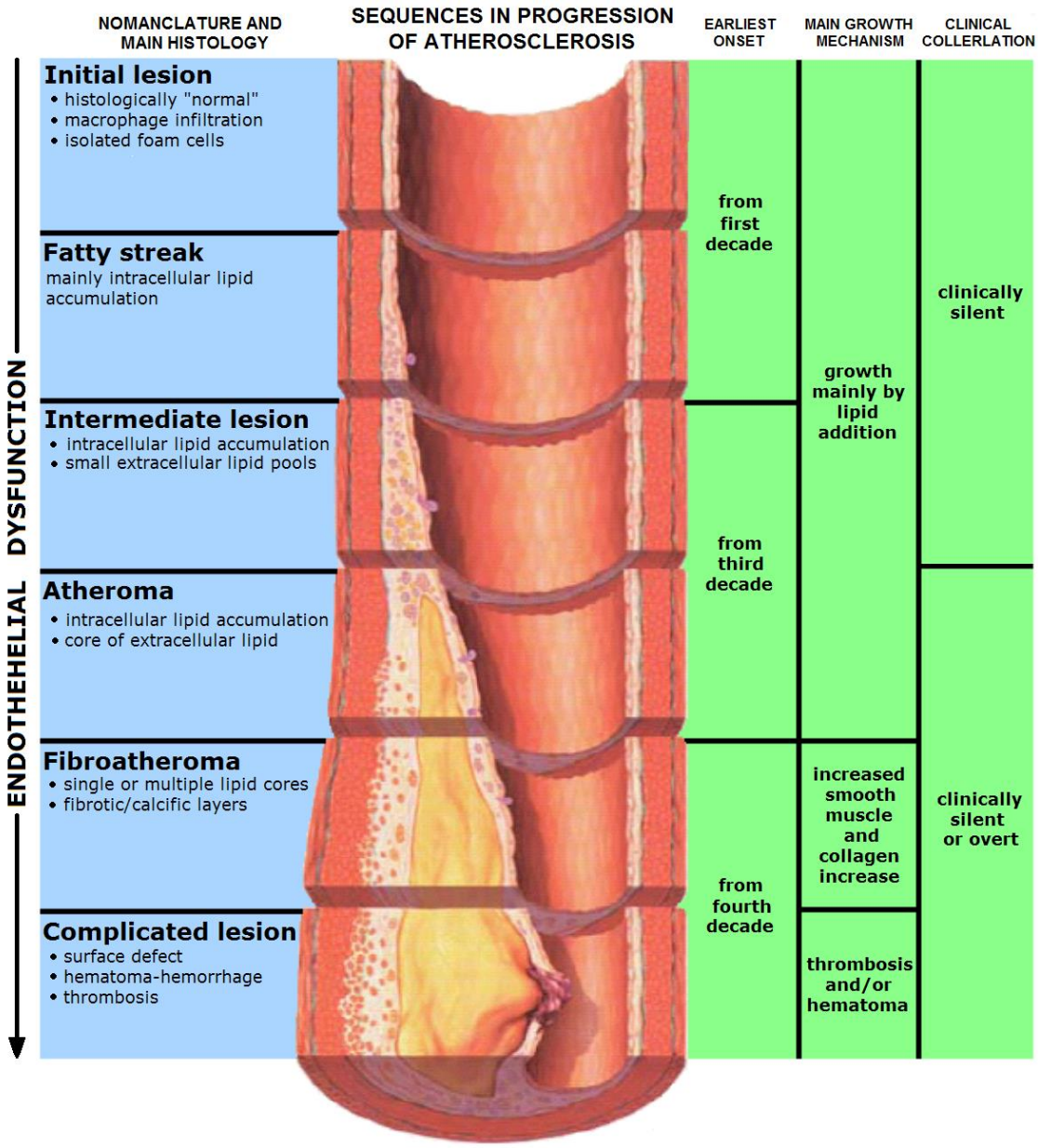

Figure 2.5:The progression of atherosclerosis (Atherosclerosis,wikipedia)

2.2.2 Recent methods to explore Atherosclerosis

Atabek (1966) considered an artery as elastic and isotropic tube and the blood inside it as Newtonian, viscous and incompressible. Element of non linearity was neglected in this study which has lead to more idealized results. Furthermore, results of longitudinal displacement of arterial wall were very large compared to the observed experimental undulation of vessel wall(Atabek and Lew, 1966).

Steady blood flow analysis was performed in coronary artery models using different blood flow models. Effect of these models on wall shear stress has been analyzed. At small inlet velocities power law model over estimates the wall shear stress whereas under estimated at high velocities. Walburn-schneck on the other hand underestimates the results of wall shear stress at high inlet velocities(Goubergrits et al., 2008). Due to these reasons both Powel and Walburn-schneck models are not widely used and are considered as unreliable (since the resultant values diverge from the correct answer) for blood viscosity modeling. Non Newtonian model in comparison was suggested as more suitable to predict wall shear stress particular at low blood velocities (Johnston BM et.al, 2004).

In another study conducted by Beulen and coworkers in 2009, blood flow was taken as laminar and incompressible.Navier-Stokes equations were used to solve the blood model whereas force-equilibrium equations were used for the solution of structure domain. Vessel wall was assumed to be as linearly elastic with limited strain. Purpose of their study was to investigate rupture risk of aneurysm and they found out that the shape of aneurysm is an important factor in fluid structure interaction for predicting the risk of rupture(Johnston et al., 2004, Beulen et al., 2009).

Specialized finite elements based algorithms were also developed for hemodynamic analysis of blood (Crossetto P, 2011).In numerical analysis proper inlet and outlet conditions were imposed. At outlet of vessel wall flux conditions obtained from 1D simulations were also applied .Finally results of FSI and CFD simulations were compared and found out that magnitude of wall shear stress is overestimated in models with rigid wall.

In a recent idealized 3D FSI study plaque rupture as a result of interaction with blood was studied (Oualid Kafi et.al, 2017). Properties of nonlinear hyper elastic material have been assigned to vessel. Result indicates that vessel wall flexibility highly affects the von Mises stress inside the plaque. Higher the flexibility more will be the chances of plaque rupture.

2.3 Attributes of Fluid Structure Interaction

To understand the mechanism of interaction between blood and vessel wall numerically it is necessary to be familiar with the attributes and approaches used to address the FLUID structure interaction.

2.3.1 Compressible vs. incompressible flow

Compressibility is a thermodynamic material property of fluids defined as measure of change in density due to pressure or temperature change. Ideal gases display such behavior. But it is to be noted that incompressible doesn't means that the fluid is itself incompressible

To some extent, all fluids are compressible but in some cases fluctuations in temperature or pressure are so minute that change in density is negligible hence we make an approximation that fluid density is constant and assume the fluid as incompressible. In other words, it can be expressed as density ρ of a fluid model does not change as it moves from one point to other within a flow field (Klainerman and Majda, 1982).

2.3.2 Viscous vs. in viscid flow

Fluids having zero viscosity are termed as in viscid fluids. If viscosity is neglected, the Navier stokes equations which are used to represent viscous flows takes form of Euler equation.Renold number of an in viscid fluid approaches to infinity.Assumtion of zero viscosity fails at interface boundaries of solid and fluid.

Viscous fluids are those fluids which are experiencing internal resistance due to friction between the layers of fluid. This internal friction is a result of cohesive forces between the molecules of fluid (Gilman, 1969).

2.3.3 Steady vs. unsteady flows

Steady flows refers to the flows in which fluid properties such as velocity, temperature, pressure, and density do not change at given point overtime. These properties however could be a function of space in steady flows. Assumption of fluid as steady is just to simplify the analysis however in real world most of the flows are transient.

Flows that are function of time are unsteady flows and can be further categorized into periodic and non periodic flows. Some flows though unsteady are assumed as steady depending upon the frame of reference. It should be noted that unsteady flows doesn't mean that velocity and acceleration is constant at a given point. There is a clear distinction between steady and uniform

flow which is just a function of space defined as “A flow in which the properties of fluid remains constant at each and every point of fluid flow”(Brater et al., 1976).

2.3.4 Laminar vs. turbulent flows

When particles of fluids follow a smooth streamline path they are said to be in a laminar flow in contrast to the flows exhibiting tiny whirlpools during is path. Generally a flow can be both laminar and turbulent, initially the particles could follow a straight line path but as speed of them increased the pattern of their motion fluctuates making the flow as turbulent. One aspect of laminar is to consider velocity constant at any given point(“Laminar Vs. Turbulent Flow”,2018).

2.3.5 Monolithic approach vs. Partitioned approach.

A monolithic or direct approach is when the equations governing the flow and the displacements of the structure are solved simultaneously in a single solver. The discretization of models leads to the generation of huge matrix of equations on which a single solver workout to find a less efficient solution than the partitioned approach in which fluid and structure equations are solved separately by two independent solvers. Many simulation suits like ABAQUS CAE have both solvers embedded within it (figure 2.6).

Partitioned approach is more useful since two distinct sets of codes are written behind the solvers to find a solution of two different domains. In addition partitioned approach requires a coupling algorithm which helps in finding the solution of coupled problem. Interaction could be either strong coupled or loosely coupled. A loosely coupled algorithm is explicit and there will be only single bidirectional exchange of solved variables per time step. But it should be noted here that explicit algorithm is suitable only when the time step taken in analysis is small enough. A strong coupled algorithm (Implicit)on the other hand uses an iterative scheme for convergence(Degroote, 2010).

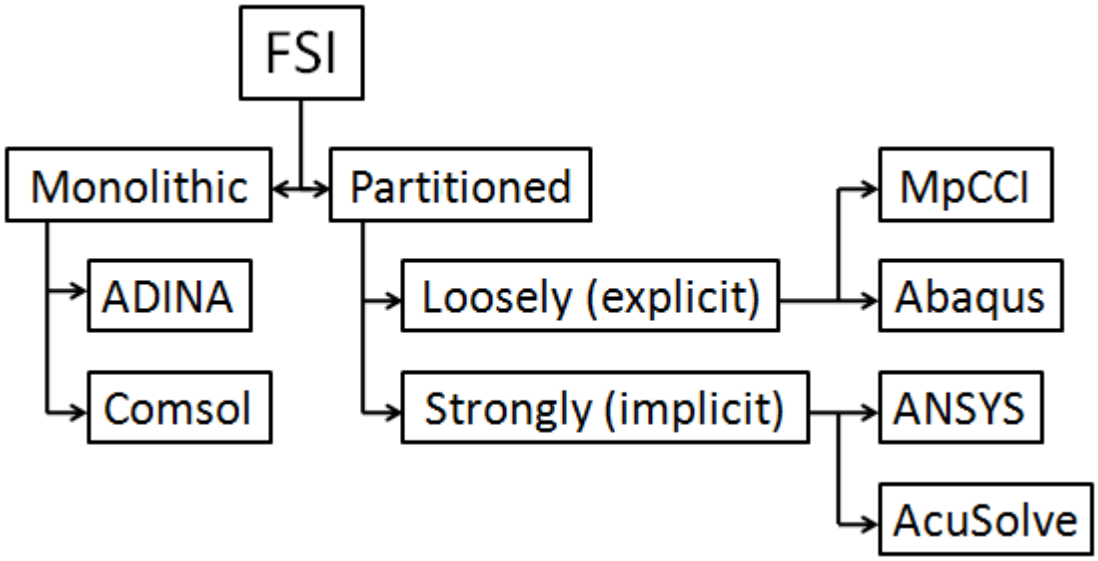

Figure 2.6:Attributes of FSI (Simulia, 2010)

2.3.6 Unidirectional vs. bidirectional coupled analysis

These both are coupling schemes used in simulation suits. If the coupling strength in one direction is so small so that the deflection of other component can be neglected than unidirectional analysis could be of use. Contrastingly, let's assume that a fluid is exerting a pressure on structure and the resulting magnitude of deflection by the structure is so large that it is back deforming the fluid element then this state requires bidirectional coupling analysis to be addressed. In ABAQUS CAE Gauss-Seidel (serial) coupling scheme is used in which one solver waits while the other solver proceeds (Figure 2.8).Abaqus/Standard or Explicit leads the simulation while Abaqus/CFD lags(Systemes, 2010).

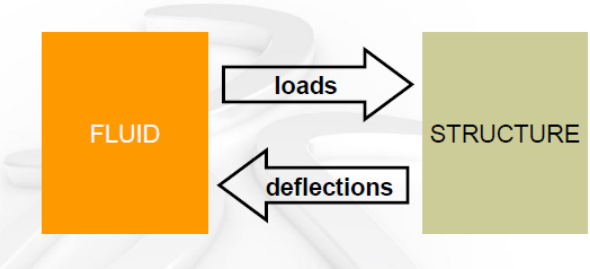

Figure 2.7:Bidirectional Coupling (Dassault Systèmes, 2010)

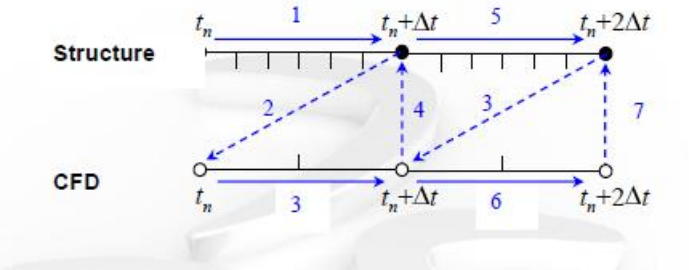

Figure 2.8:Gauss- Seidel coupling (Dassault Systèmes, 2010)

2.4 Coronary Artery Calcium Scoring

Calcium is an essential element found in living organism. Beside bones and teeth arteries are also prone to the augmentation of calcium. Although calcification of the arteries is a part of aging phenomenon but extensive calcium is thought to be related with some specific stages of atherosclerosis (AHA, 2000). These calcium spots in coronary arteries are collectively termed as calcified plaque (Figure 2.9) and a technique to calculate their score in coronary artery is called coronary artery calcium (CAC) scoring. This score is an individual marker for early risk prediction of cardiac events. The purpose here is to associate mechanical strength of an artery with its corresponding calcium score to find out the amount of calcium contributing to a particular plaque burden in an artery.

Hounsfield unit (HU) is a scale to measure density of the object. Calcified plaque has HU value greater or equal to 130HU in a standard 120kvp scans (NA-MIC, 2014). Calcium score (aka Agatston score) is calculated based on the area and peak ct value of a single calcium spot

Table 2.1 and 2.2 are showing X factor (page.) intensity ranges and Agatston score characterization.

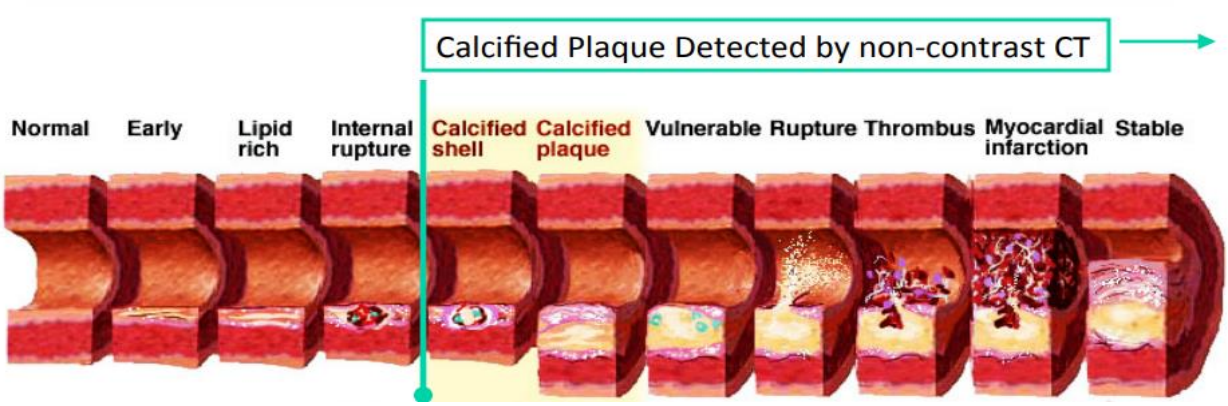

Figure 2.9: Coronary arterial calcification; part of atherosclerosis development

Table 2.1: HU Ranges and their corresponding X factors (NA-MIC,2004)

HU Range	**X Factor**
130-199 HU	1
200-299HU	2
300-399HU	3
=>400HU	4

Table 2.2: Agatston Score Ranges and Prognosis (NA-MIC 2014)

Total Agatston Score	**Prognosis**
0	No Identifiable disease
1-99	Mild Disease
100-399	Moderate Disease
=>400	Severe Disease

2.5 Role of Mechanics in Vasculature

Mechanical balance within vasculature is critical to their normal functioning. Blood Flow within blood vessels makes them expose to various mechanical forces such as shear stresses, longitudinal stresses, strains and deformation (Kwak et al., 2014).

Coronary arteries are one of those arteries which are seriously affected by the lumen blood pressure. Endothelium cells are those cells of vasculature that lines the interior surface of blood vessels (Figure 2.10). These cells live in a dynamic environment due to the hemodynamic of

blood flow. Mechanical stimuli experience by these cells includes shear forces due to contact with blood, strain due to pressure distension of wall and deformation due to increased luminal pressure and owing to the fact that these blood vessels are tethered to surrounding tissue bed .These stress and strain experienced by the vessel walls causes the initiation of atherosclerosis. Mostly atherosclerosis occurs at the branch points of vessels (Warboys et al., 2011). There are many studies that confirm that these plaque deposits break mechanical damage and causes buckling of the vessel walls (Han et al., 2013). Buckling in the blood vessels along with plaque burden increased overall stress in the walls and may lead to plaque rupture which in turn causes partial or complete occlusion of blood vessel.

In healthy blood vessels, which are devoid of plaque deposits, measurement of von mises stress predicts the areas which are highly prone to develop atherosclerosis. In diseased models these stresses are important to calculate overall plaque burden to the vessel walls.

Literature indicates that areas where shear stresses are low are more likely to develop plaque lesions(Dhawan et al., 2010). These low shear-stress areas could be compared and confirmed by high von mises stress areas to predict plaque vulnerable locations.

Strain is defined as the relative change in position of points within a body that has undergone deformation. A tensor is a multi-dimensional array of numerical values that can be used to describe the physical state of material . In this study the strain component which is being considered is Logarithmic strain, because of nonlinear nature of analysis.

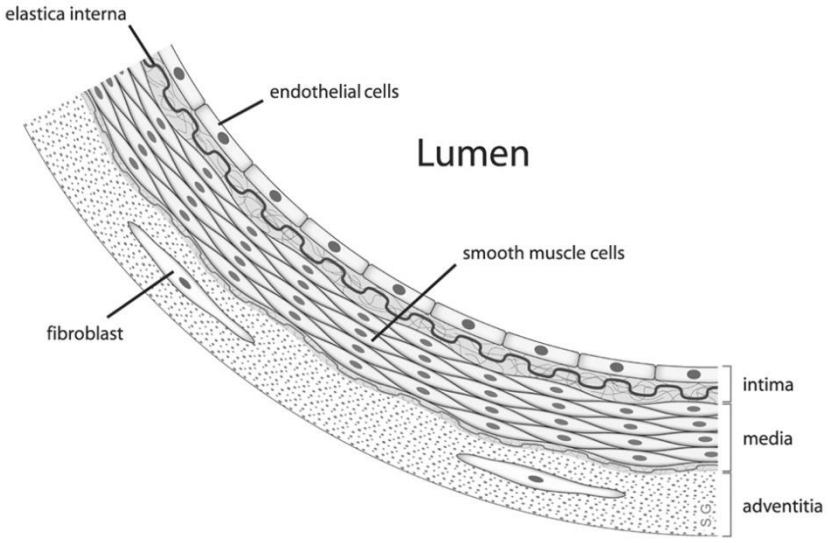

Figure 2.10: Cells of Vasculature(Endothelial cells,wikipedia)

CHAPTER 3: METHODOLOGY

Overview

This chapter presents the strategy and techniques adopted to gain insights into the mechanism of arterial deformation due to blood flow in the presence of plaque. The chapter has been divided into three major sections. Starting with the specification of medical images; reconstructions of models through segmentation from CT images are presented. This is then followed by mesh generation of both structure and fluid part. Numerical simulation of Fluid Structure Interaction is described later. The chapter closes with the validation of Fluid Structure Interaction Results with the structure based simulation approach.

Workflow

The workflow of study is shown in figure 3.1.

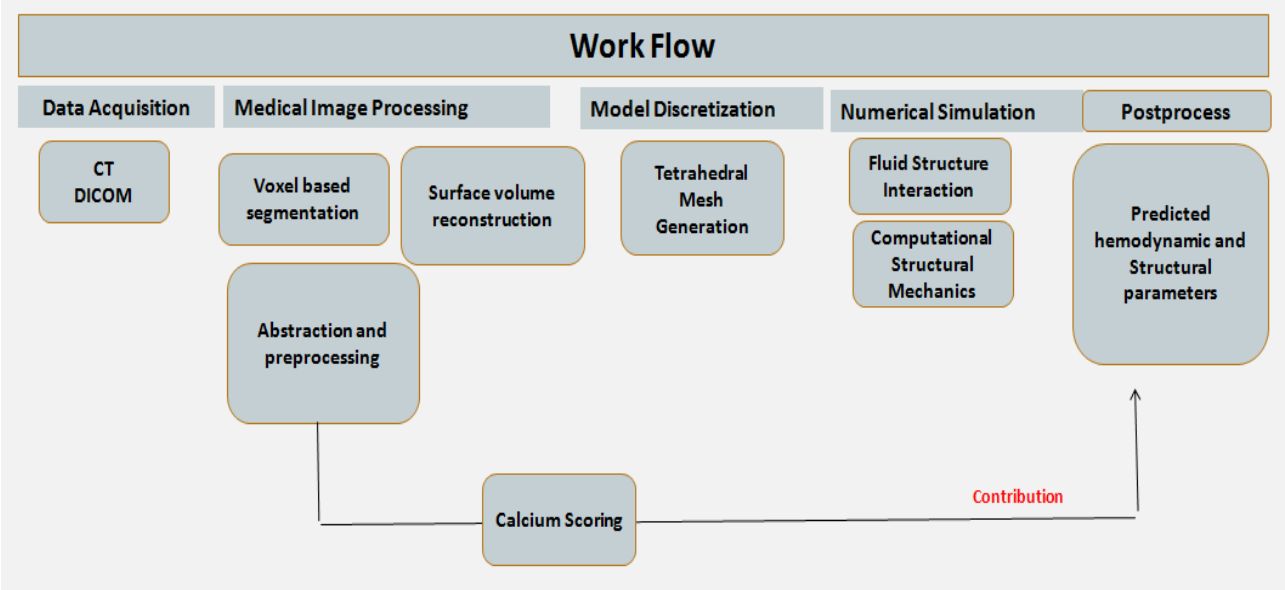

Figure 3.1: Workflow Diagram

3.1 Image Based Modeling

3.1.1 Dataset Acquisition

Both normal and patient specific dataset was obtained from an online database-Cardiac Fat database-Computed Tomography. The datasets are heart scans and of CT modality. Each dataset consist of 44 CT slices and acquired in 2014 using Philips ict 256 CT scanner.

Normal heart scan is of a 52 year old Male weighing 71 kg. Scans are in DICOM (Digital Imaging and Communications in Medicine) format having slice thickness of 3mm with voxel size of 0.3066×0.3066×3mm^3 and a resolution of 3.2611 pixel per mm.

Whereas diseased dataset belongs to a 53 year old male (Figure 4.1). The resolution of dataset is 2.8444 pixel per mm and the voxel size is 0.3516× 0.3516× 3mm^3.

3.1.2 Segmentation and Model Reconstruction

Both models were segmented using Mimics Materialise 17.Segmentation was done based on Hounsfield units (HU). Rodrigues et al. (2015) defined an interval range of (-200,-30) HU for cardiac adipose tissue within CT scans. So the interval we have taken to access the adventitia of right coronary artery is (-200, 29) accepting the fact that anatomically adipose tissue is contiguous with the adventitial layer of the blood vessel wall (Chatterjee et al., 2009).Figure 3.2 is depicting anatomic location of adventitia.

Calcified plaque was segmented using a CT threshold of ≥130 HU involving 3 contiguous voxels (Budoff et al., 2010).Fibrous plaque was manually segmented and its range of Hounsfield units were found to be (90-129HU) which is in relation with the literature (Schroeder et al., 2001) (Figure 4.3-4.4). A napkin ring pattern corresponds to the fibrous plaque tissue has also been identified with the spotty calcification within the rim (Figure 3.3).Figure 4.2 (A-D) are showing steps for separating Right Coronary Artery from rest of Heart's substructures.

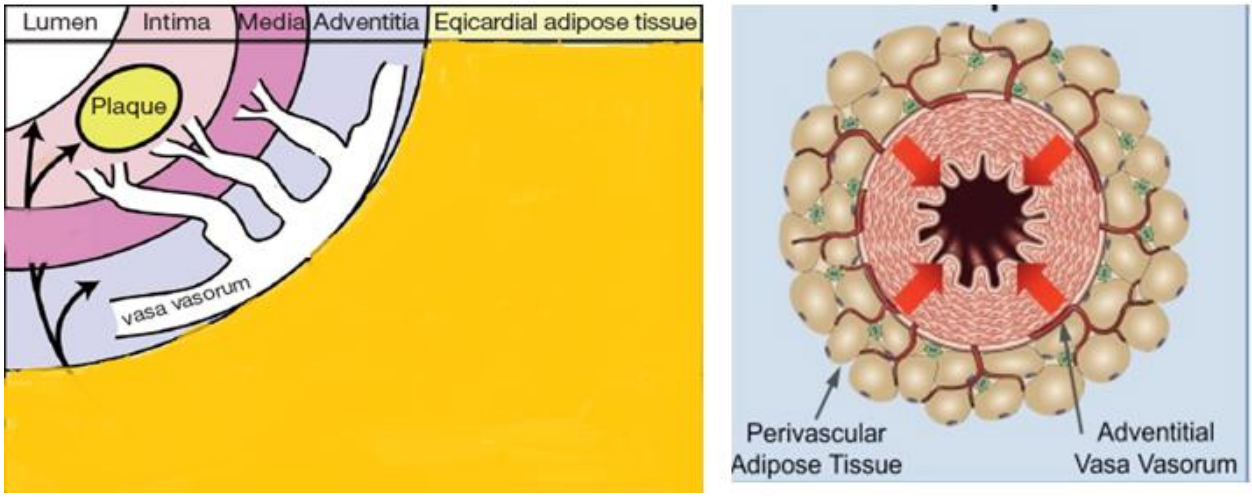

Figure 3.2:Location of Adventitia in Blood vessel (Talman et al., 2014)

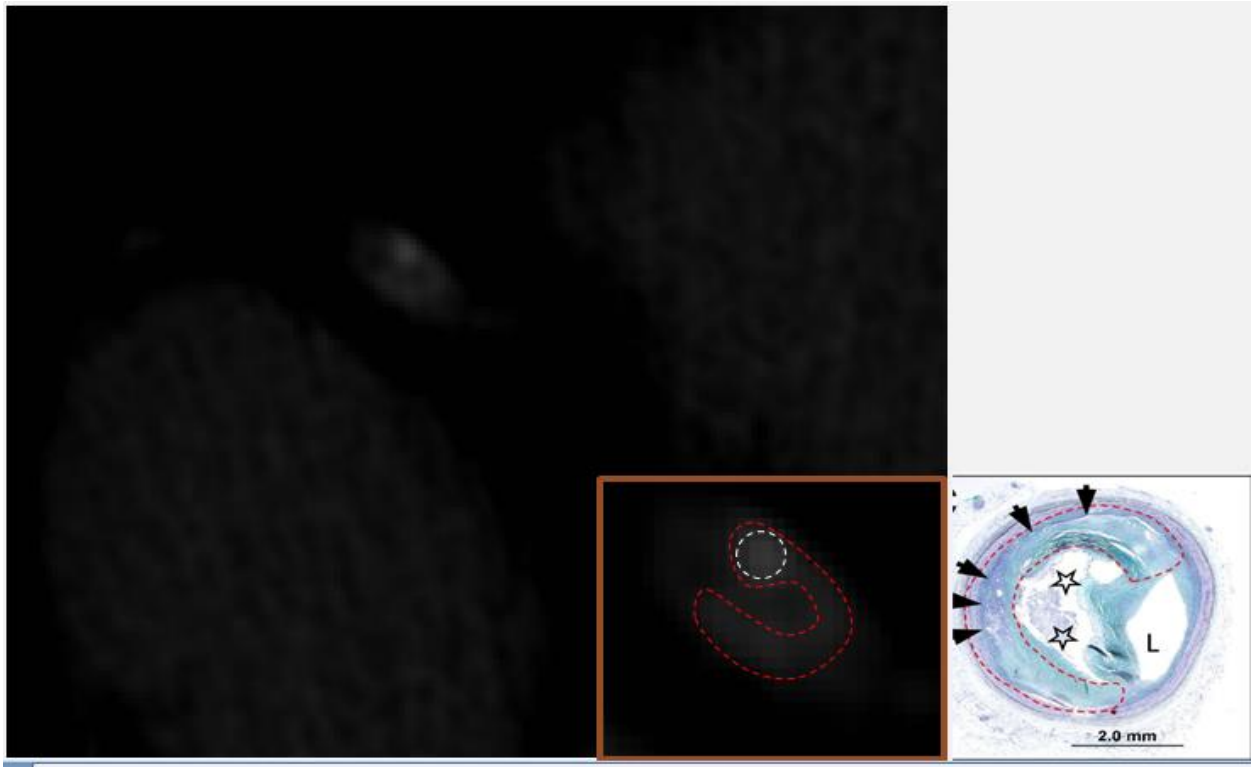

Figure 3.3: Napkin-Ring sign

3.1.3 Mesh generation and Mesh Convergence Analysis

The segmented models were imported in 3matic and a smoothing filter was applied to make the surface of the model more regularized. Other filters applied are listed in table 3.1. The artery was made hollow by moving its outer boundaries 0.4mm inside so that the lumen can fix inside it. Figures 4.5-4.6 in chapter 4 are showing segmented volume, surface mesh and volume mesh of both normal and diseased patients.

Some manual editing (Figure 4.7) was also required to create tetrahedral error-free meshes 4.7.Figure 3.4 is showing 3-matic report regarding accuracy of Mesh. To test whether further increase in mesh size will affect the results or not, mesh convergence was carried out using varying edge lengths (Figure 4.9). Mesh size and their respective edge lengths are shown in table 3.2.

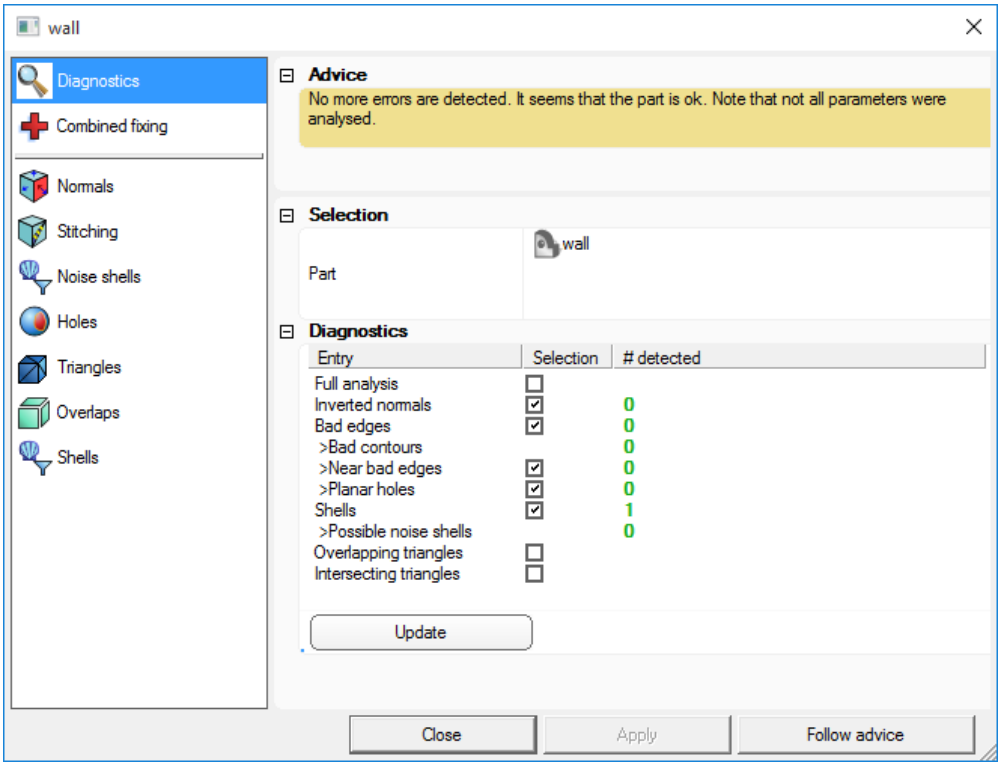

Figure 3.4:Mesh Accuracy check by 3 Matic

Table No 3.1: Manual and Automatic Operation performed to generate the mesh.

Operations Performed	**Function**
Gaussian Filter	Smoothing
Automatic Fixing	Optimize the mesh
Centerline Extraction	Separate centerline from substructures of heart
Boolean Intersection/Subtraction	Ensure separation of masks
Global Registration	Co-register the models
Hollow	Gives a thickness to wall of artery
3D Multiple edit	Model edit at volume level
Manual surface mesh tools	Refine single element
Remesh	Transform bad quality triangles into equilateral triangles
Adaptive Remeshing	Improve surface mesh locally

Table No. 3.2: Mesh Convergence Analysis

Models	Components	Edge length	No. Of elements	Total elements	Displacement Mm
1	Wall (Structure)	0.5	71705	439784	2.166
	Lumen (CFD)		368079		
2	Wall	0.4	204323	930982	3.348
	Lumen		726659		
3	Wall	0.3	462858	2198596	3.71
	Lumen		1735738		
4	Wall	0.2	1729567	7604770	3.799
	Lumen		5875203		

3.2 Numerical Analysis

Numerical methods are those problem solving techniques by which mathematical problems are formulated so that they can be solved using arithmetic operations. These methods are generally used to solve extremely complex real world phenomenon where higher degree of non-linearity is involved.

Complicated problems like Fluid structure interaction which couples Navier stokes equations of fluid with momentum and equilibrium equations of structure are solved through these numerical methods.

Traditional fluid flow simulations don't take interaction into account. But today, to get an accurate and better understanding of these intricate systems it is no longer possible to ignore the boundaries between different physical domains.

3.2.1 Fluid Structure Interaction

Numerical Analysis is divided into two approaches. First FSI method is described in detail while procedure of structural analysis is presented in the later part.

3.2.1.1 Fluid Mechanics

ABAQUS/CFD was used for the finite element analysis of fluid structure interaction.

Blood flow was assumed to be laminar, Newtonian, viscous and incompressible. The fluid domain was handled using Arbitrary Lagrange-eulerian (ALE) solver. This solver is widely used

for blood flow analysis in vessel walls. Material properties that were used for blood are shown in table 3.3.

Boundary Conditions for Fluid part

The fluid has been divided into three components that are inlet, outlet and wall. Velocity of 0.2 m/s is applied at inlet while a pressure of zero has applied at outlet and no slip condition at wall has imposed (Figure 3.5(A)). Courant-Friedrichs-Lewy (CFL) number was set to 0.45. CFL number is chosen usually for the timestep size and is broadly used for the stability of unstable simulations. Appropriate initial and Final "Step time" was chosen as and are listed in the table 3.4.

Velocity at Inlet of Blood Model $\rightarrow u|inlet = u\ velocity$

Pressure at Outlet $\rightarrow \sigma\ nn|outlet = 0$

3.2.1.1.1 Governing Equations of Fluid Part

Mass and Momentum conservation equations for an incompressible fluid is represented below

$$\boldsymbol{\nabla . V = 0} \quad (1)$$

$$\boldsymbol{\frac{\partial V}{\partial t} + (V.\nabla)V = \nu \nabla^2 V} \quad (2)$$

where,

$$\boldsymbol{\nu = dynamic\ velocity}$$

$$\boldsymbol{\frac{\partial V}{\partial t} = fluid\ velocity\ w.r.t\ time}$$

Table No. 3.3: Material Properties of Arterial Components(Nagy, 2010)

Components	Density (Kg/m^3)	Hyper elastic Material Constants (Pa)		Viscosity (Pa.s)
		C10	C01	
Blood	1050			.00345
Wall	1000	9200	3600	
Calcium	1000	92000	36000	
Fibrous	1000	9200	666	

Table No. 3.4: Step Duration assigned to Finite Elements Simulation(Oscuii et al., 2007)

		Step Duration	Initial step time
Normal	Structure	0.2	0.002
	Fluid		0.002
Diseased	Structure	0.0002	0.000002
	Fluid		0.000002

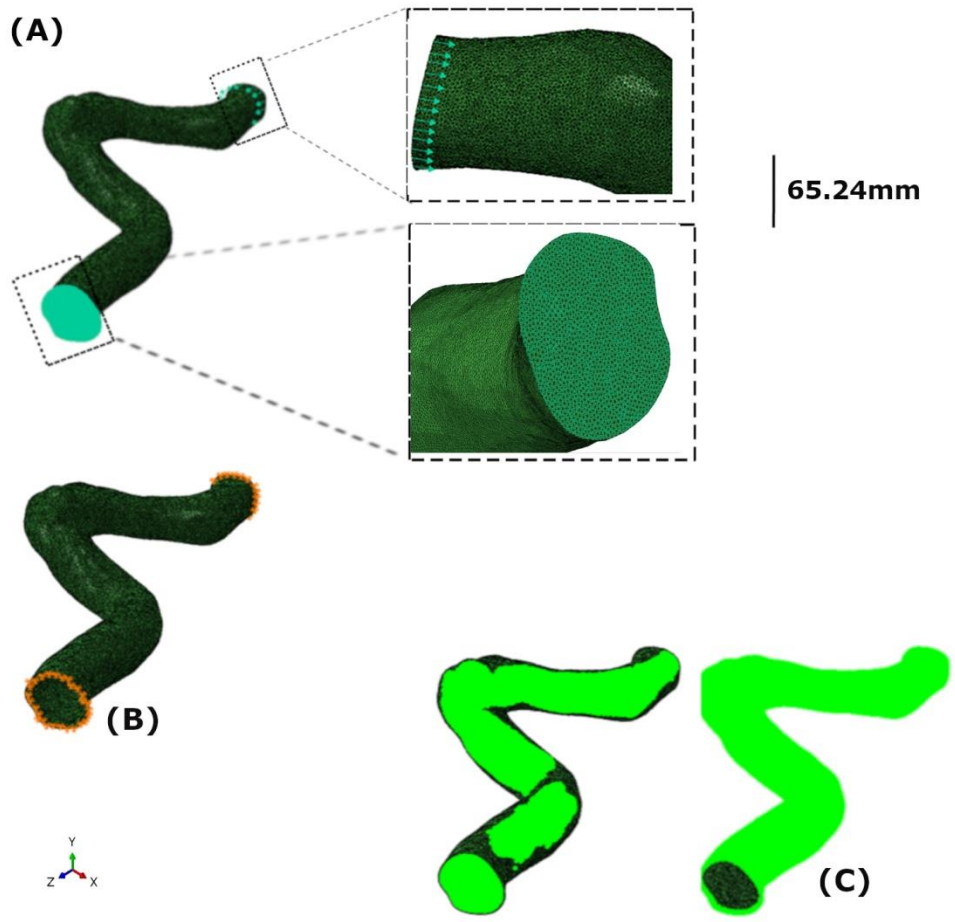

Figure 3.5:A) Inlet velocity of 0.2 m/s and pressure drop at outlet has imposed as boundary conditions on blood domain.(B) Encastre vessel ends.(C) Interaction surfaces of solid and fluid

3.2.1.2 Solid Mechanics

ABAQUS Standard/Explicit was used for structural part handling in fluid-structure interaction. Arterial wall and plaque components were assumed to be of Neo-hookean material type.Neo-hookean is a hyperelastic material model that can be used for predicting the nonlinear stress-strain behavior of materials undergoing large deformations.It's a modified form of Mooney Rivilin material model.

The form of neo-Hookean strain energy potential is

$$U=C10\ (\bar{I}1-3)+1/D1\ (J^{el}-1)^2, \quad (3)$$

where,

U = strain energy per unit of reference volume;

$\bar{I}_1$ = first deviatoric strain invariant defined as $\bar{I}_1 = \bar{\lambda}^2_1+\bar{\lambda}^2_2+\bar{\lambda}^2_3$

J^{el} = elastic volume

In ABAQUS the parameters of neo-Hookean material model are expressed in terms of c10 and D1. Provided the shear modulus (mu) and the bulk modulus (kappa) the values of these variables can be derived by using the formula mentioned below

$$C10=mu/2$$

$$D1=2/kappa$$

Material Properties of both Blood and Wall are represented in Table 3.3.

Boundary conditions for solid part

The vessel wall has four surfaces inlet, outlet, outer surface and inside surface of vessel. Inlet and outlet of an artery were kept fixed for both translation and rotations.

Inlet=Outlet=ENCASTRE

Figure 3.5 (B) is representing boundary Conditions applied at vessel wall

3.2.1.2.1 Governing Equations of Solid Part

Momentum conservation equation for the mechanical behavior of solid is represented by

$$\nabla.\sigma s = \rho s Ug \quad (4)$$

Where,

$\rho s = solid\ density$

$\sigma s = stress\ tensor$

$Ug = local\ acceleration\ of\ solid$

3.2.1.3 FSI coupling

Navier stokes equation for the fluid and momentum as well as equilibrium equations for solid are coupled with the fluid solid interface via the dynamic condition. The nodes of both solid and fluid part must coincide at the FSI interface. The Arbitrary Lagrangian-Eulerian (ALE) method was employed to couple the solid (arterial wall) and fluid (blood) nodes together.

To create an interaction between solid and fluid part outer wall surface of blood model and inner surface of vessel wall was chosen (Figure 3.5 (c)).

Boundary Conditions needs to satisfied at interface

(1) Displacement of both Fluid and Structure must be compatible.

$$\delta s = \delta f \tag{5}$$

(2)Traction at this boundary must be in equilibrium.

$$\sigma s.\hat{n}s = \sigma f.\hat{n}f \tag{6}$$

(3)Fluid must obey the "No-slip" condition at the interface.

$$u = ug \tag{7}$$

where,

∂ =displacement

σ = Stress tensor

$\hat{n}$ =Boundary Normal

and the subscripts f and s are indicating a property of fluid and solid property.

3.2.2 Structure analysis

FSI study has been validated through structure analysis. In structure analysis exclusively, the only difference with respect to model creation is that lumen is not taken into account and all space within vessel wall except plaque components was assumed as lumen.

Finite elements simulation analysis was performed in Abaqus-standard/explicit. No interaction was defined instead assembly of all structural components is created.Additionally, instead of velocity; mechanical pressure of 14600 Pa is applied at internal surface of wall as shown in Figure 3.6.

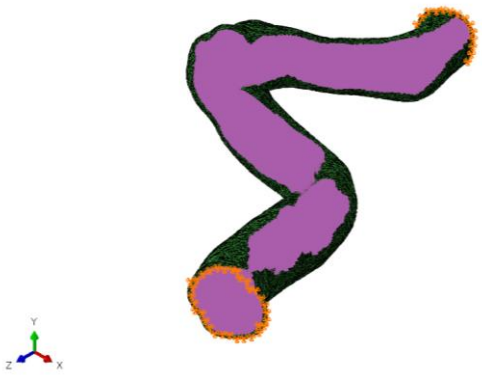

Figure 3.6:Boundary Conditions of Structure based Analysis

Figure 31-44 are showing the results of Numerical simulation

3.3 Calcium Scoring

Agatston score is a semi-automated tool to determine extent of coronary calcification normaly detected by an unenhanced CT scan. To calculate Agatston score python script was utilized. Scripting was done in console of 3D slicer, a software for three-dimensional visualization and image processing. The software first performs automatic segmentation based on the given threshold followed by scoring of calcified spots.Agatston score is the product of area covered by a single spot and its corresponding X factor.X factor is a value assigned to a particular intensity range (Table 2.1). Total Agatston score of a single vessel is a sum of individual scores. An increased Agatston score predicts an increased risk of coronary events(Budoff et al., 2013). Based on literature in different studies a chart has been drawn(Table 2.2) that relate coronary artery calcium score to the extent of atherosclerotic coronary artery disease.

CHAPTER 4: RESULTS

In this study Finite element analysis is carried out to simulate the mechanical behavior of healthy and atherosclerotic coronary artery in response to underlying blood flow. The primary focus is to analyze the stress-displacement behavior of arteries in response to the internal luminal pressure. Comparably, lesion-free walls are exhibiting more deformation than the atherosclerotic artery having more rigid wall, allowing very minute displacement. This is due to the fact that plaque deposits have hardened the arterial walls overtime. Similarly Von Mises stress magnitude is high in diseased model because of the severe stenosis which makes the blood to flow with high speed thereby generating great magnitude of pressure in the obstructed region. Shear stress is varying inversely proportion with the vessel wall flexibility. Furthermore low shear stress zones could be compared to the high von Mises stress areas to confirm the future risk of plaque development in healthy model.

4.1 Image Based Modeling Results

Image processing phase is further divided into sections as described below:

4.1.1 Data Acquisition

Data was acquired, as explained in chapter 3 section (3.1.1). Figure (4.1) shows the results of the acquired data.

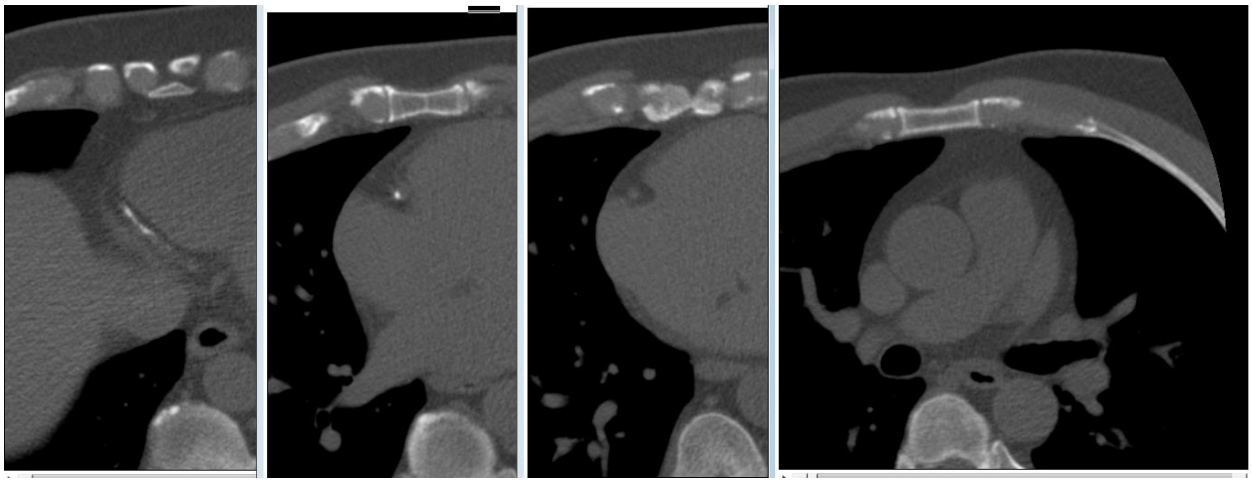

Figure 4.1:Four slices of cardiac CT showing calcified plaque in coronary artery.

4.1.2 Segmentation and model Reconstruction

Figure 4.2 (A-D) is illustrating the stepwise segmentation of coronary artery components.

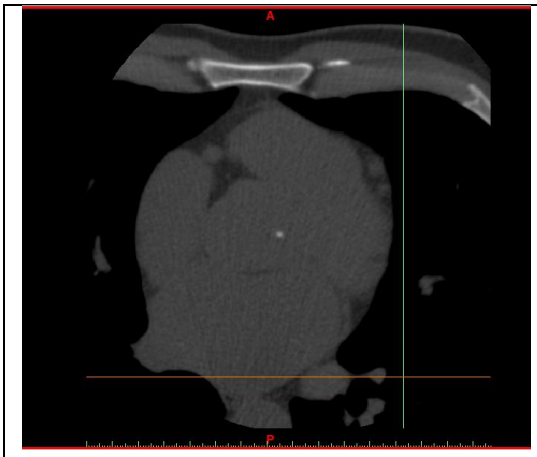

Figure 4.2-A: Dicom image

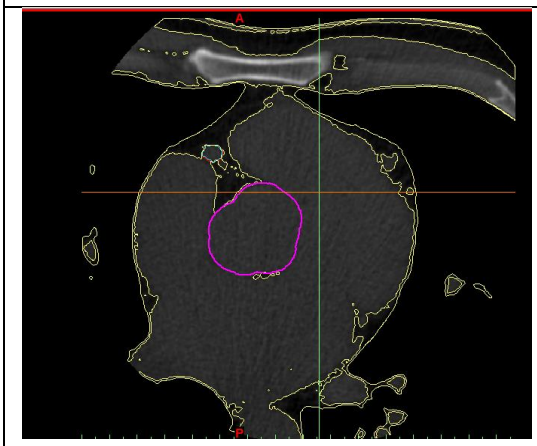

Figure 4.2-B: Boundary tracing and Edge Detection

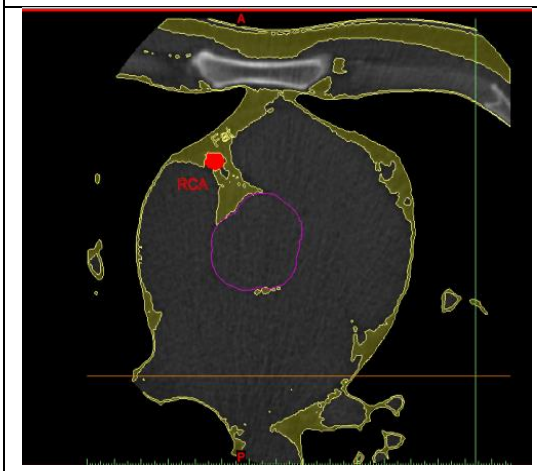

Figure 4.2-C: Separating Right Coronary Artery

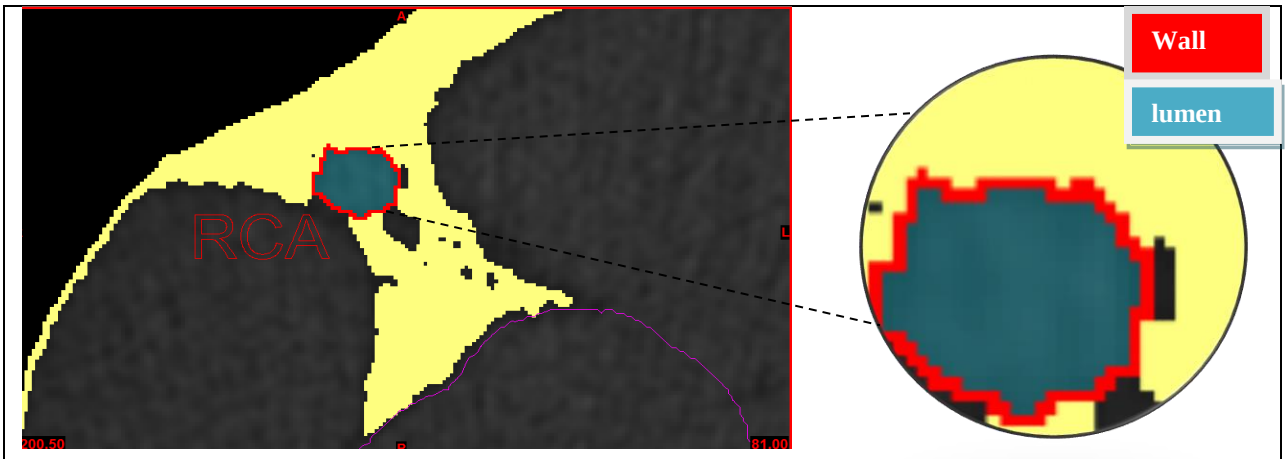

Figure 4.2:Coronary Artery Segmentation

Figures 4.3-4.4 are showing the segmented plaque components based on Hounsfield units as described in section 3.1.2 of chapter 3

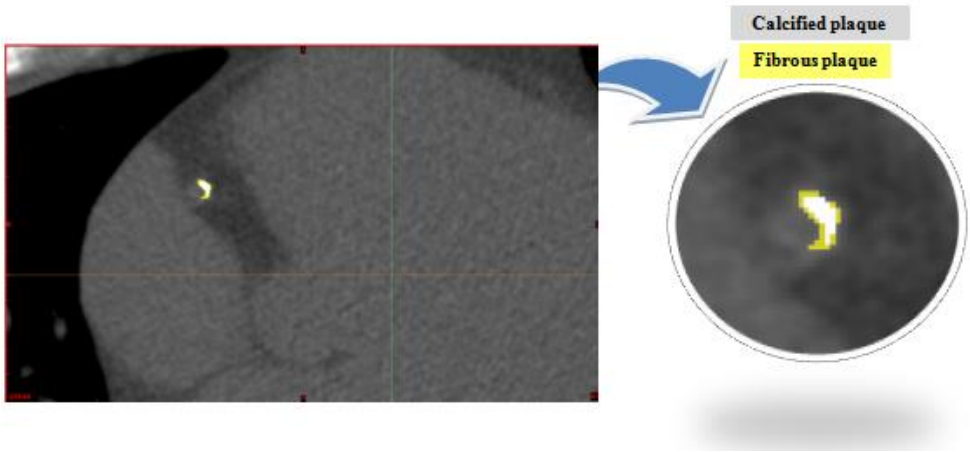

Figure 4.3:Segmented plaque on 2D image

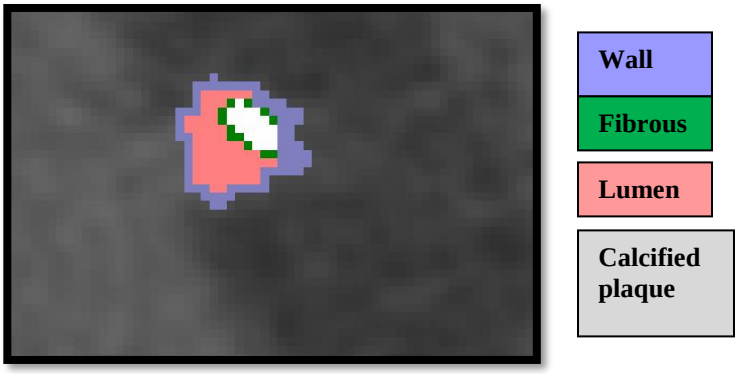

Figure 4.4:Segmented components of an artery

4.1.3 Mesh Generation and Mesh Convergence Analysis

Figure 4.5 is showing the segmented volumes and meshes of the models used for FSI. However Figure 4.6 is representing the models used for structure based analysis.

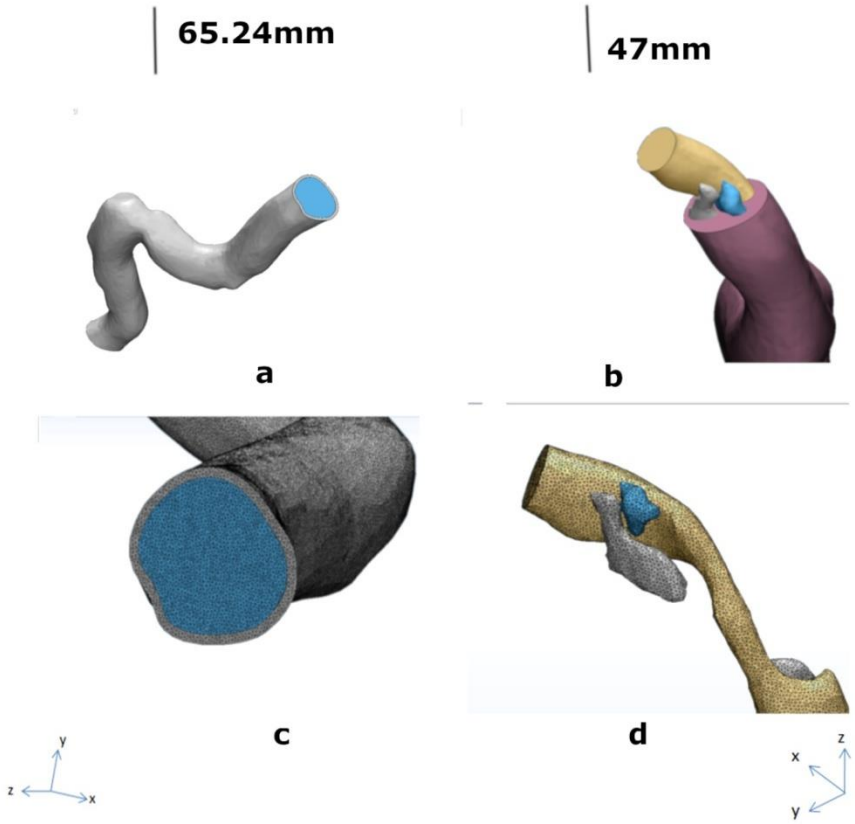

Figure 4.5:(a) Segmented volume of healthy artery. (b) Segmented volume of diseased vessel. (c) Healthy model mesh. (d) Atherosclerotic vessel mesh.

Figure 4.6-A:Wall Model of Structural Analysis

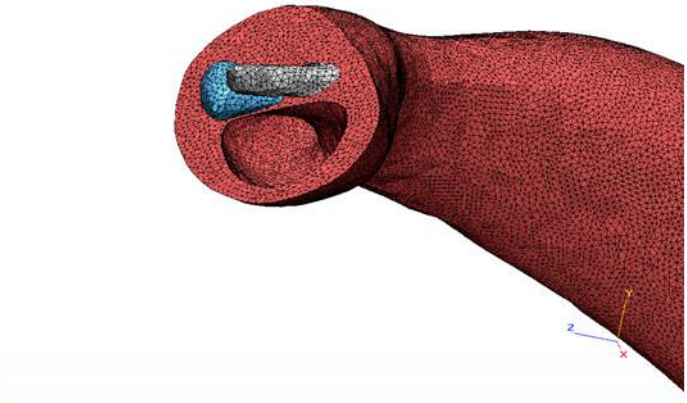

Figure 4.6-B: Volume Mesh of Structural Components

For further mesh refinement ‘Adaptive Remeshing’ which is a built-in mimics operation was performed.

Figure 4.7:Adaptive Remeshing

There is a built-in automated centerline extraction method in Mimics, Materialise with some manual adjustment options to further characterize tubular structures. These centerlines are powerful descriptors of dimensions and shape of vessels.

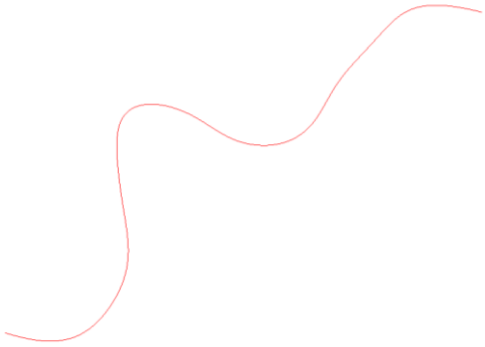

Figure 4.8:Centerline Extraction

Results are more accurate with the finer mesh. To attain that precision mesh convergence was carried out. Figure 4.9 is showing the mesh density of four different wall models. The graph in Figure 4.10 is explaining the relation between mesh density (of four models with different edge length) and deformation. It can be seen that further increase in mesh density will no longer affect the deformation results. Hence the fourth model (having 7604770 total elements) is the converged one.

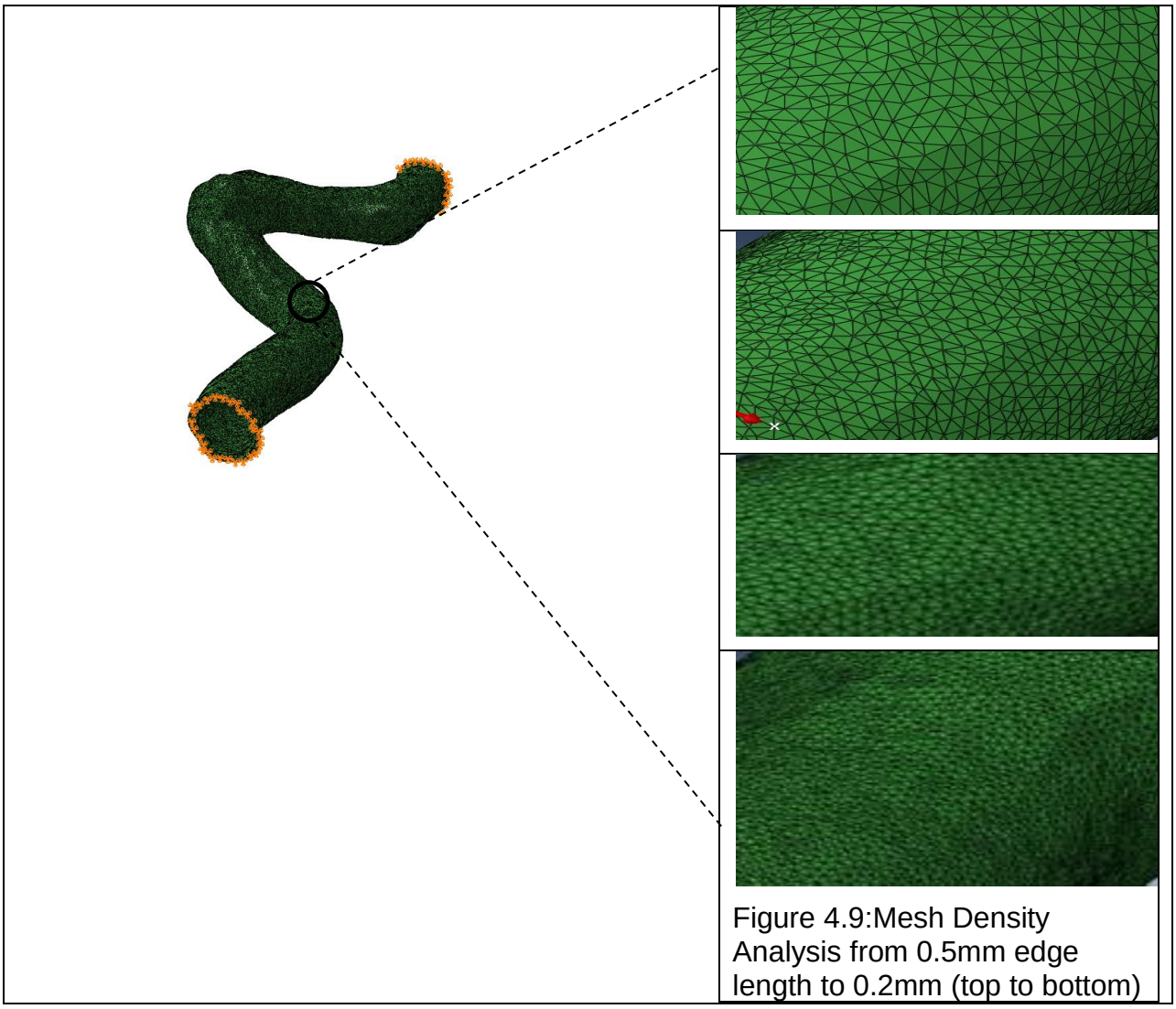

Figure 4.9:Mesh Density Analysis from 0.5mm edge length to 0.2mm (top to bottom)

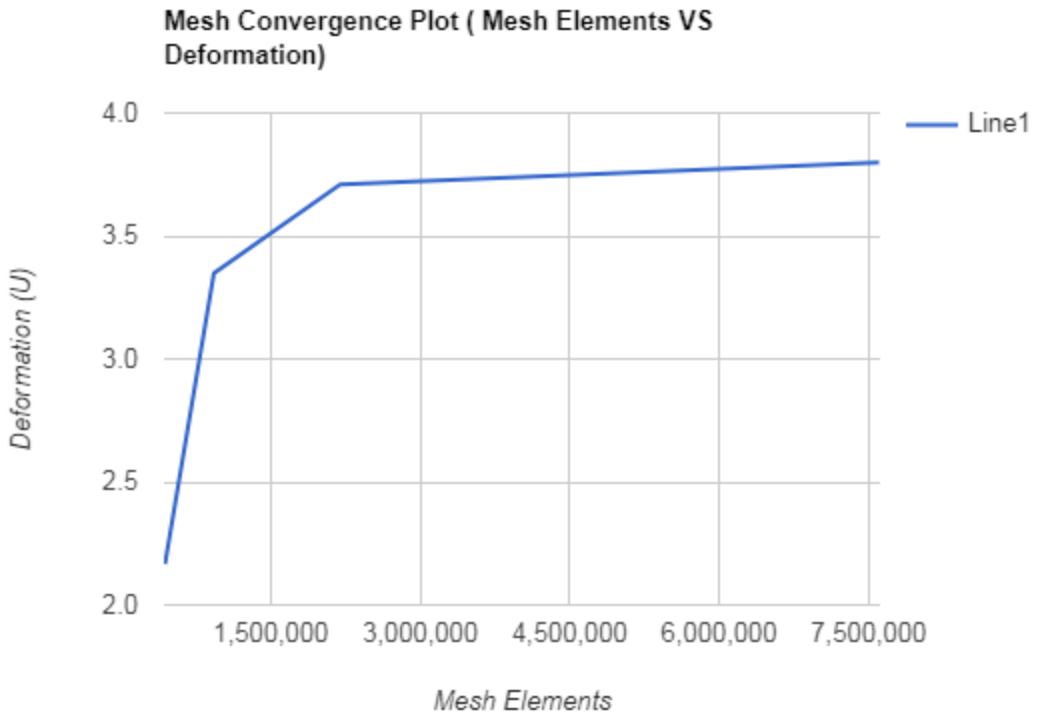

Figure 4.10:Mesh Convergence Graph

4.2 Numerical Analysis Results

In this section simulation results of Healthy and Atherosclerotic artery using both fluid Structure Interaction and Structure based approach are described.

4.2.1. Deformation (U)

4.2.1.1 Deformation of Arterial Wall

i. Fluid Structure Interaction

In Healthy model Deformation (U) using FSI approach ranges from 0-3.799 mm (Figure 4.11) (Torii.R et all, 2009).Contour plot legend is aligned in descending order (from Maximum (red) to

Minimum (blue)). Maximum deformation is seen on the final converged model (Figure 4.11(D)) which corresponds to the finite element size of 0.2 mm.

Deformation contours are distributed from the inlet till the distal bend of artery (which is 3/4 of its length)(Figure 4.11(D)). Deformation is maximum at the intrados of proximal bend which is under compressive loading whereas zero at the outlet where 'pressure drop' has imposed as a boundary condition. The increased curvature at proximal bend may cause buckling because at this wrinkled location majority of the deformation associated with the loading has concentrated.

In diseased model the deformation ranges from 0 to 5.9 mm (Figure 4.12(a)). It is zero at the inlet and outlet of wall structure where the model was kept fixed (Translation=Rotation=0). Deformation contours are distributed along the inner lining of vessel wall at the surface of endothelium and has travelled to the outer coat near the inlet and outlet (Figure 4.12(a)). Narrow region of lumen also falls in the interval of legend representing maximum deformation.

i. Structure based Analysis

Healthy model deformation ranges from 0 to 1.6 mm (Figure 4.13).Deformation contours are distributed over the whole surface of wall from internal to external surface. 'Zero' deformation can be seen at both inlet and outlet of vessel wall. These are the points where the model was "*encastred".*

In the diseased model the deformation ranges from 0 to 0.0596mm (figure 4.12(b)).Deformation contours are distributed inside vessel wall at the interface of lumen and wall. The reason for this equal distribution is an internal pressure of 14600 Pa that has been applied to all nodes present at the surface of endothelium. It is zero at the inlet and outlet of wall structure where the model was kept fixed.

Walls of healthy models are free from any deposition of plaque components so they have retained their elasticity as compared to the diseased rigid one hence the name *Arteriosclerosis* – 'Arterio' means arteries and 'scleorosis' means hardening (loss of elasticity).There are more chances of healthy model to undergo plastic deformation than diseased model which permits a low level of displacement.

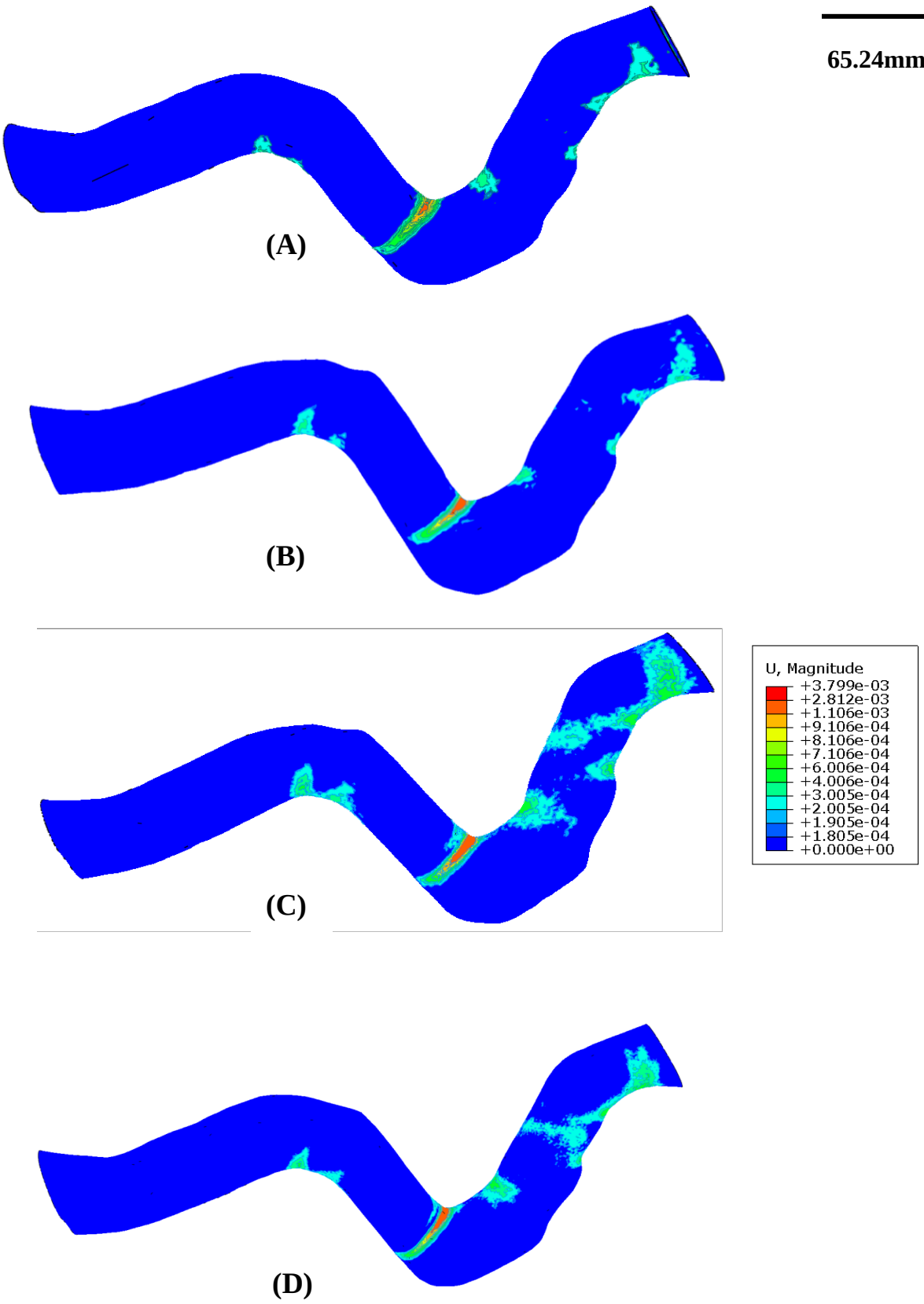
65.24mm
(A)
(B)
(C)
(D)
U, Magnitude
+3.799e-03
+2.812e-03
+1.106e-03
+9.106e-04
+8.106e-04
+7.106e-04
+6.006e-04
+4.006e-04
+3.005e-04
+2.005e-04
+1.905e-04
+1.805e-04
+0.000e+00

Figure 4.11: Deformation plots on Healthy model using FSI approach.(A) Model with finite element size of 0.5mm.(B) Model (edge length:0.4mm).(C) Model (edge length:0.3mm).(D)Model (edge length:0.2mm) showing maximum deformation at the intrados of bend.

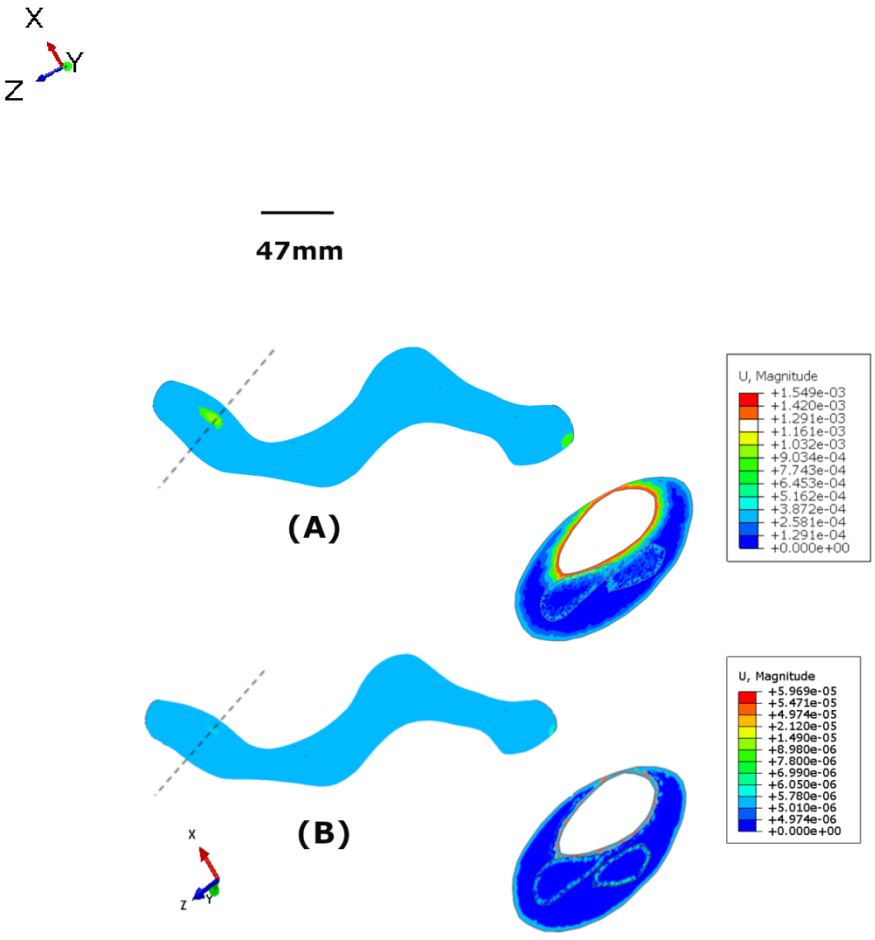

Figure 4.12: Deformation plots on diseased artery using FSI (top) and Structure based approach(bottom).

Figure 4.13: Deformation (U) Plots on Healthy Model showing distributed deformation using Structure based approach.

4.2.1.1 Deformation of Plaque Components

Figure 4.14 is showing Deformation contours on plaque components. Maximum deformation on fibrous plaque is recorded as 3.612e-9 mm and that of calcified plaque is 2.301e-8 mm, which is almost negligible numerically however at a micro scale, responsible for quite a lot of disruption.Hence fibrous plaque here is predicted to be more stable than calcified plaque deposits. Although majority of publications are claiming calcified plaque as more stable than soft plaque but it should be noted that the debate about whether calcifications stabilize plaque is still open. A recent study(de Kreutzenberg et al., 2015) also has confirmed a progressive rise in the risk of cardiovascular events with increasing plaque calcification.

Greater the stability less will be its vulnerability. The results indicate that calcified plaque may be due to its location and geometry is more prone to rupture (deformation: 2.301e-8 mm) while the fibrous plaque is exhibiting the stiffest response (3.612e-9 mm) to the high strain loading.

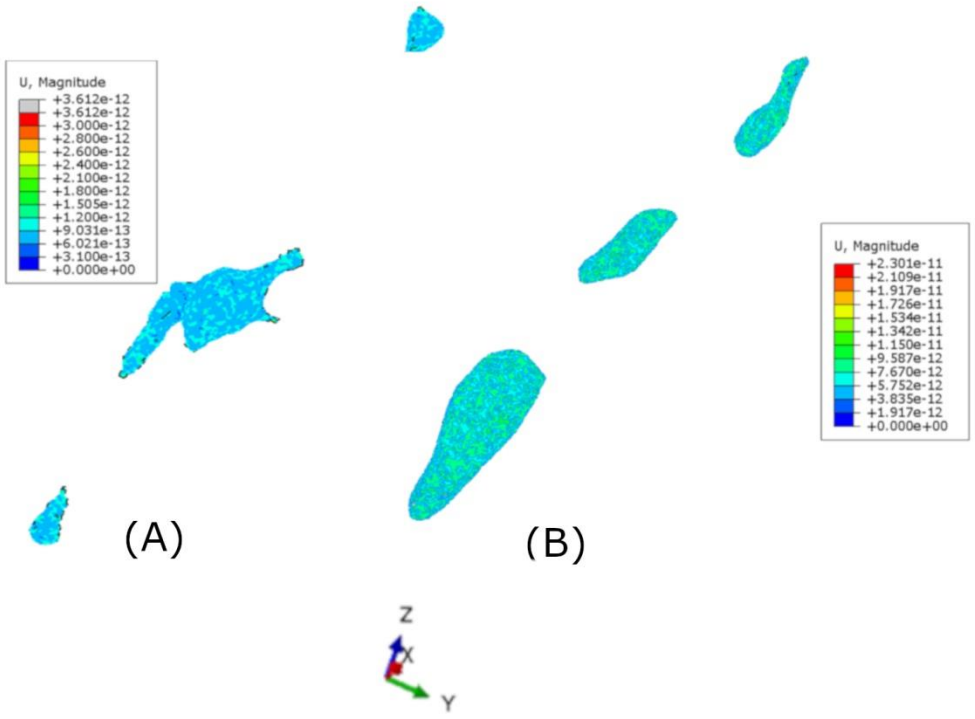

Figure 4.14: Deformation (U) plots on fibrous plaque and calcified plaque

4.2.2 Stress

4.2.2.1. Von Mises Stress

FSI

Figure 4.15 shows four models from courser to finer. Model D corresponds to the model with an element size of 0.2mm.It shows maximum stress which is 516.3 Pa. Stress contours are dispersed across the artery from proximal to distal end with maximum stress at the intrados of largest curvature where compressive residual stresses are concentrated.

Increased Von Mises Stress (Figure 4.15(D)) at inner curvature of bend makes this site more vulnerable to plaque development. Hence if we predict the future risk of atherosclerosis for this model, this is the place where plaque is likely to form.

Maximum Stress in the diseased model using FSI approach is 94720.0 Pa and least is 5.683e-15 Pa and stress contours are distributed inside the artery along the inner lining of vessel wall where lumen is in contact with the wall (Figure 4.16).At some sites particularly in the vicinity of inlet and outlet, deformation contours has travelled from the endothelium surface to the outer surface of adventitia.

Structure based Approach.

Maximum stress experienced by the wall of healthy model using structure based approach is 237.0 Pa (Figure 4.17). However contours for maximum stress are not localized at one place, they are distributed across the artery with the maximum stress at the interface (where lumen meets wall).The reason for these scattered contour is the homogenous application of internal pressure to the nodes present at the surface of endothelium.

Whereas using structural approach the stress scale ranges from 0-577.5 Pa (Figure 4.18). Maximum stress falls towards ends of artery (near inlet and outlet).Stress Contours are distributed along the inner lining of vessel wall.

The reason for increased stress in the diseased model might be due to the occlusion of the artery. Narrowing of the blood vessel causes the blood to impart large amount of pressure on the wall hence generating a great amount of stress especially at the areas where passage for the flow of blood is narrow causing more constrictions and increased pressures.

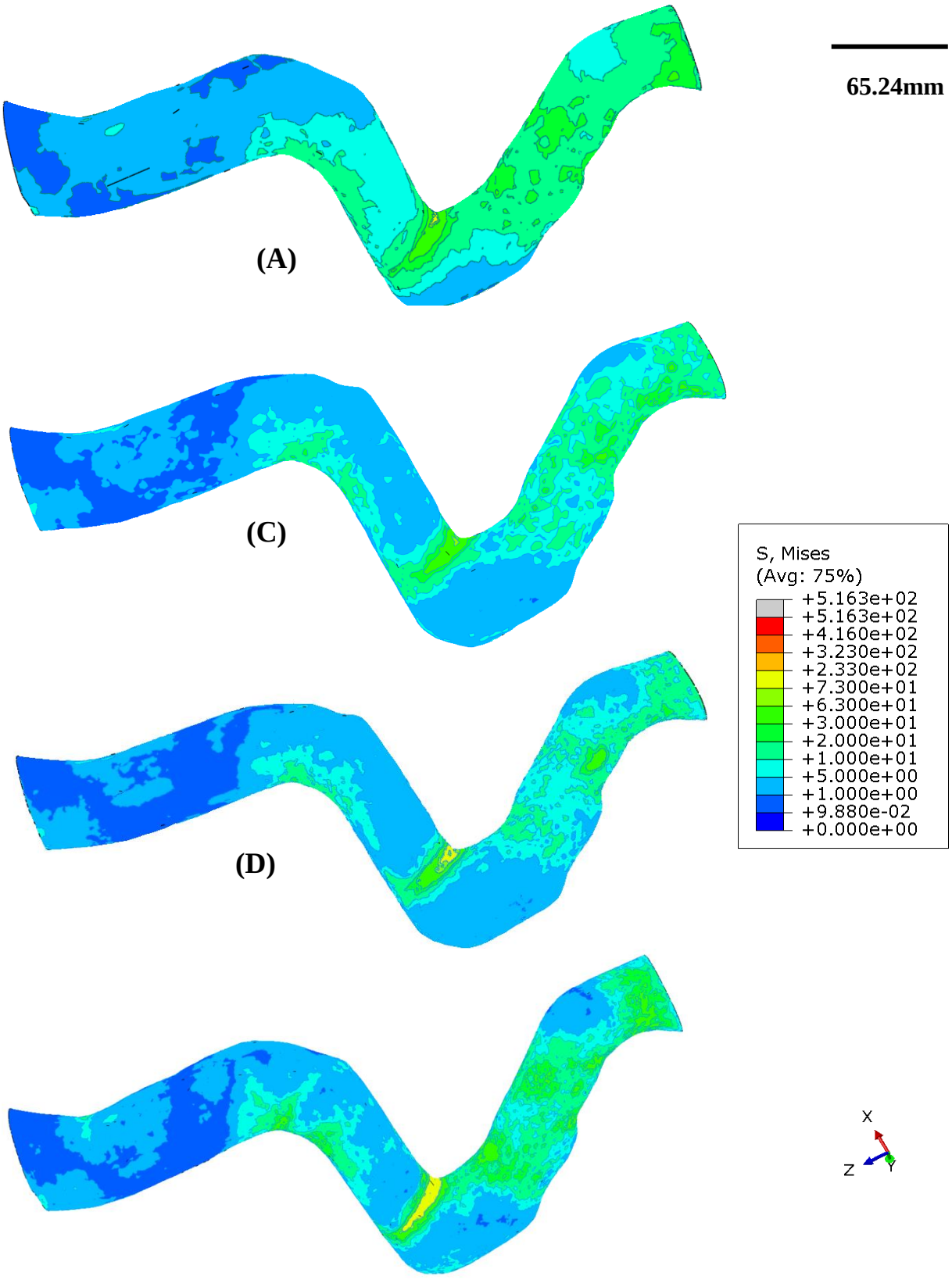
65.24mm
(A)
(C)
(D)
S, Mises
(Avg: 75%)
+5.163e+02
+5.163e+02
+4.160e+02
+3.230e+02
+2.330e+02
+7.300e+01
+6.300e+01
+3.000e+01
+2.000e+01
+1.000e+01
+5.000e+00
+1.000e+00
+9.880e-02
+0.000e+00
X
Z
Y

Figure 4.15: Von Mises Stress plots on Healthy model using FSI approach.(A) Model with finite element size of 0.5mm.(B) Model (edge length:0.4mm).(C) Model (edge length:0.3mm).(D) Converged Model (edge length:0.2mm) showing maximum stress along the inner curvature of bent.

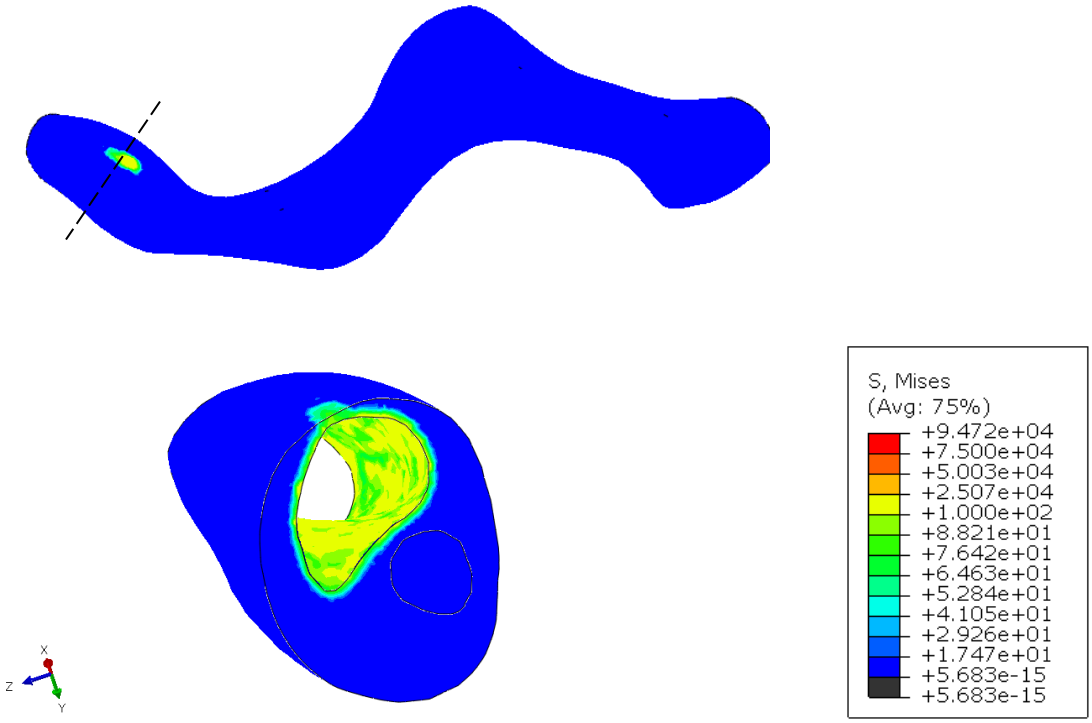

Figure 4.16:Von Mises Stress plots on Diseased artery using FSI Approach representing maximum deformation of 94720 Pa in the vicinity of inlet.

Figure 4.17:Von Mises Stress Plots on Healthy Model using Structure based approach showing distributed stress.

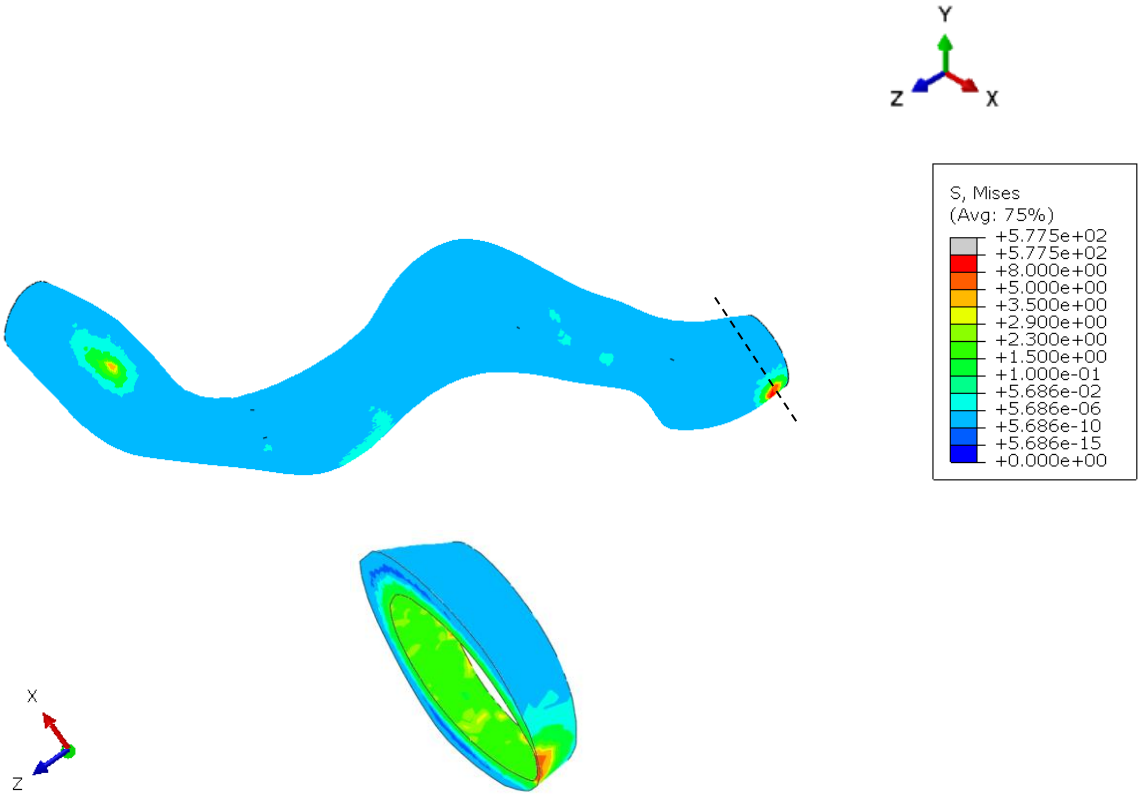

Figure 4.18:Von Mises Stress plots of Diseased Artery using Structure Based Approach showing maximum stress of 577.5 Pa somewhere in the red zone.

4.2.2.2 Shear stress

At higher shear rates the Red Blood Cells disaggregate, become elongated and gets deformed (their long axis aligns in the direction of flow), thereby minimizing the viscosity. At high shear rates blood flow behavior is Newtonian, but at lower shear rates it is non Newtonian. Generally shear stresses are measured at the boundary between forward and reverse flow.

In Healthy model minimum shear stress location corresponds to the area where von Mises stress shows maximum stress(4.19(a-b)). This confirms the fact that low shear stress areas are actually more liable to the formation of plaque. However, in diseased model maximum shear stress is distributed along the whole length of an artery inside the vessel wall with maximum stress around the end points (Figure 4.20 a-b).

Shear Stress Results confirms the fact that wall shear stress reduced with the flexibility of vessel wall. Higher the elasticity of wall less would be the magnitude of shear stress. The reason of high shear stress in diseased model is the stiffness of vessel wall due to the underlying plaque deposits.

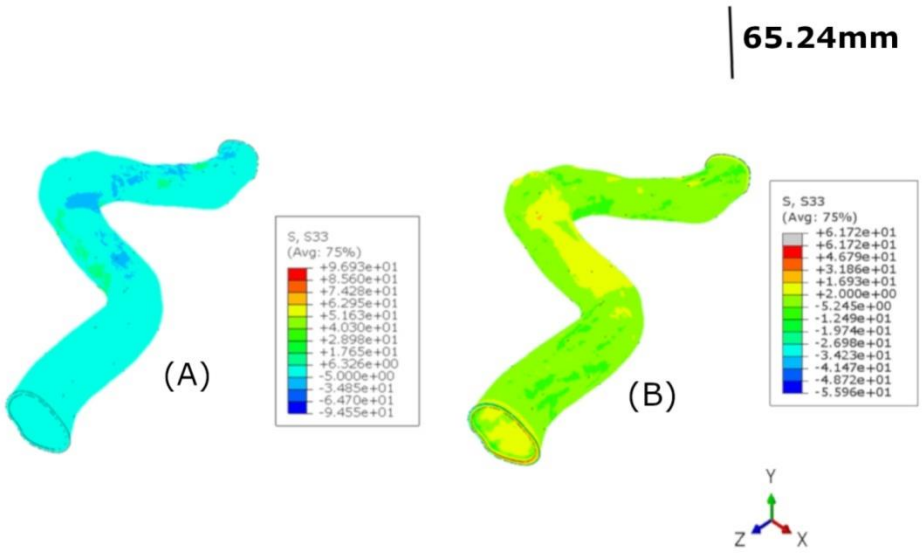

Figure 4.19:Shear Stress plots on healthy vessel using FSI (A) and Structure based approach (B).

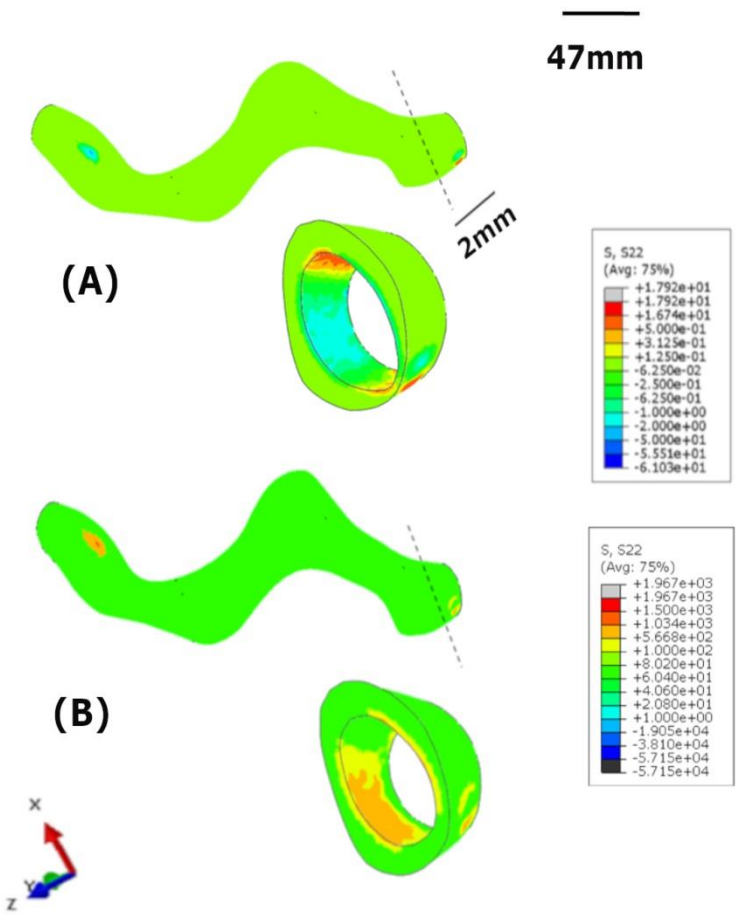

Figure 4.20: Shear Stress plots on diseased vessel using Structure based approach (A) and FSI (B).

4.2.3 Strain

Legends in figure 4.21-4.24 are showing a comparison of the strain tensors in three dimensions using both FSI and structure based approach. Overall the results of Structure based approach is showing a slight decrease in strain values as compared to results of FSI.

FSI

In Normal model, out of six dimensions yy is showing Maximum strain rates(Figure 4.21) whereas in diseased model maximum strain falls in yz direction(Figure 4.23). In Healthy artery strain contours are distributed over the whole surface of vessel wall with maximum magnitude at the wrinkle location of inner curvature where majority of deformation also took place.However

in diseased artery strain contours just lies over the surface of endothelium with some spots at outer adventitial coat as well near outlet and inlet(Figure 4.23).

Structure analysis

In normal model maximum strain lies in yz dimension (Figure 4.22) whereas in diseased model it occurs at xx dimension(Figure 4.24).In healthy model strain contours are distributed across the whole artery from inner endothelium to outer adventitial coat.In Diseased model maximum strain lies near the proximal and distal end of artery.

Results of FSI approach are more close to the literature(Kural et al., 2012, Ooi et al., 2012).

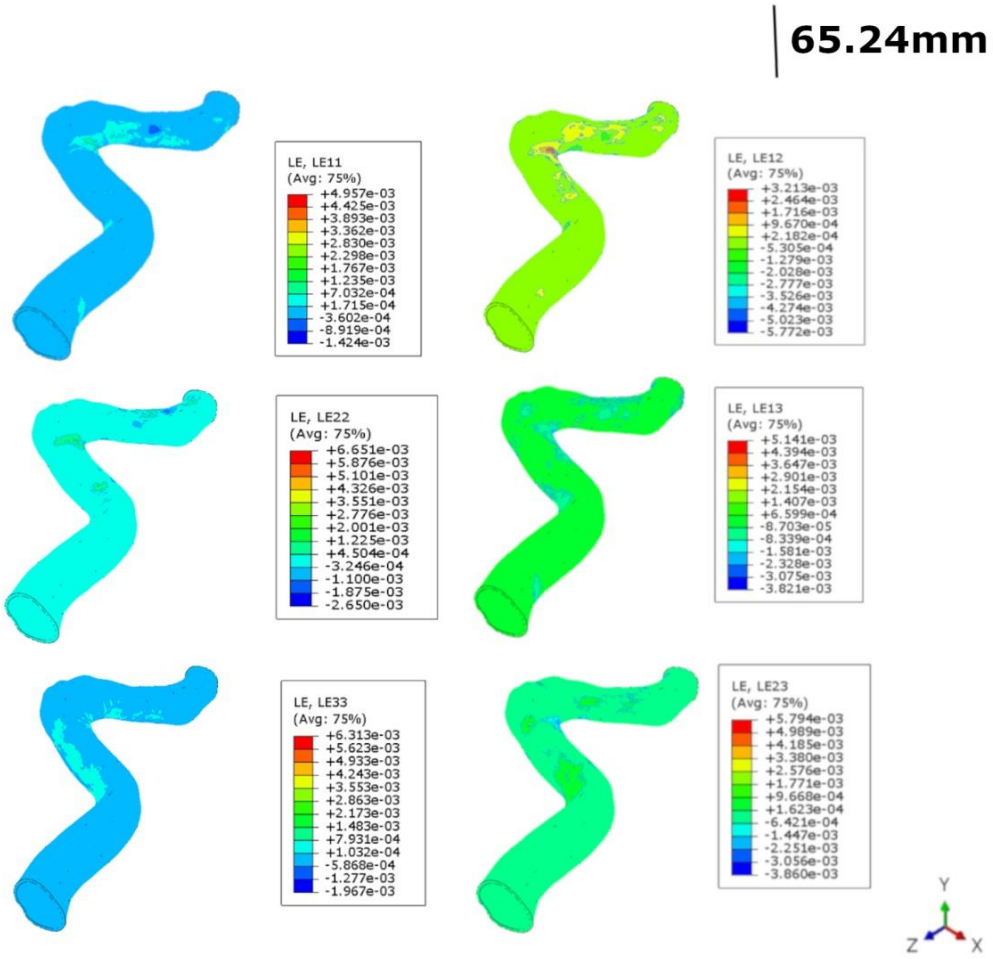

Figure 4.21: Logarithmic Strain rates on Healthy model using FSI approach in six dimensions(11=xx,22=yy,zz=33,12=xy,13=xz,23=yz),showing maximum strain magnitude in yy dimension.

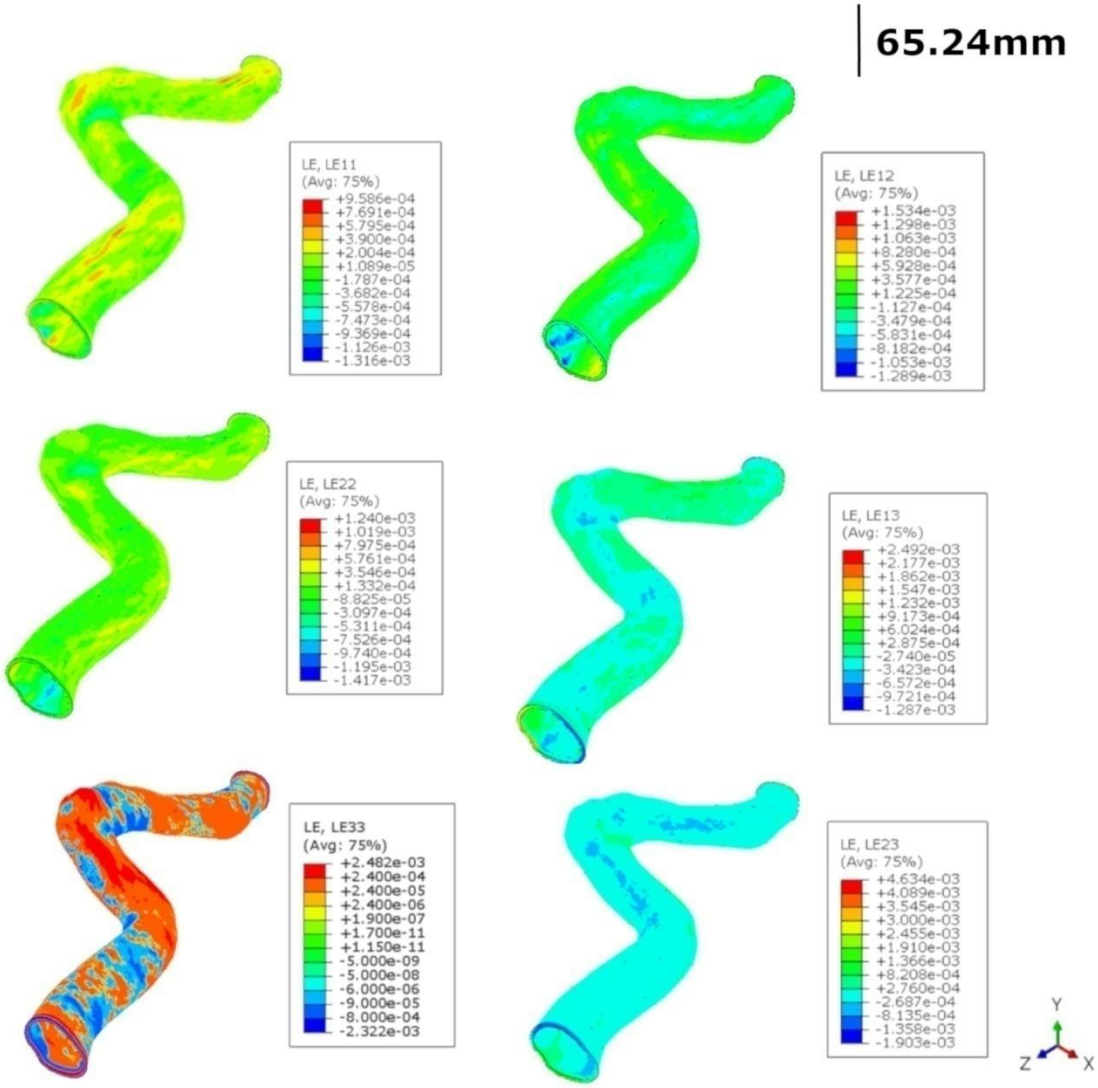

Figure 4.22: Logarithmic Strain rates on Healthy model using Structure based approach in six dimensions(11=xx,22=yy,zz=33,12=xy,13=xz,23=yz),showing maximum strain magnitude in yz dimension..

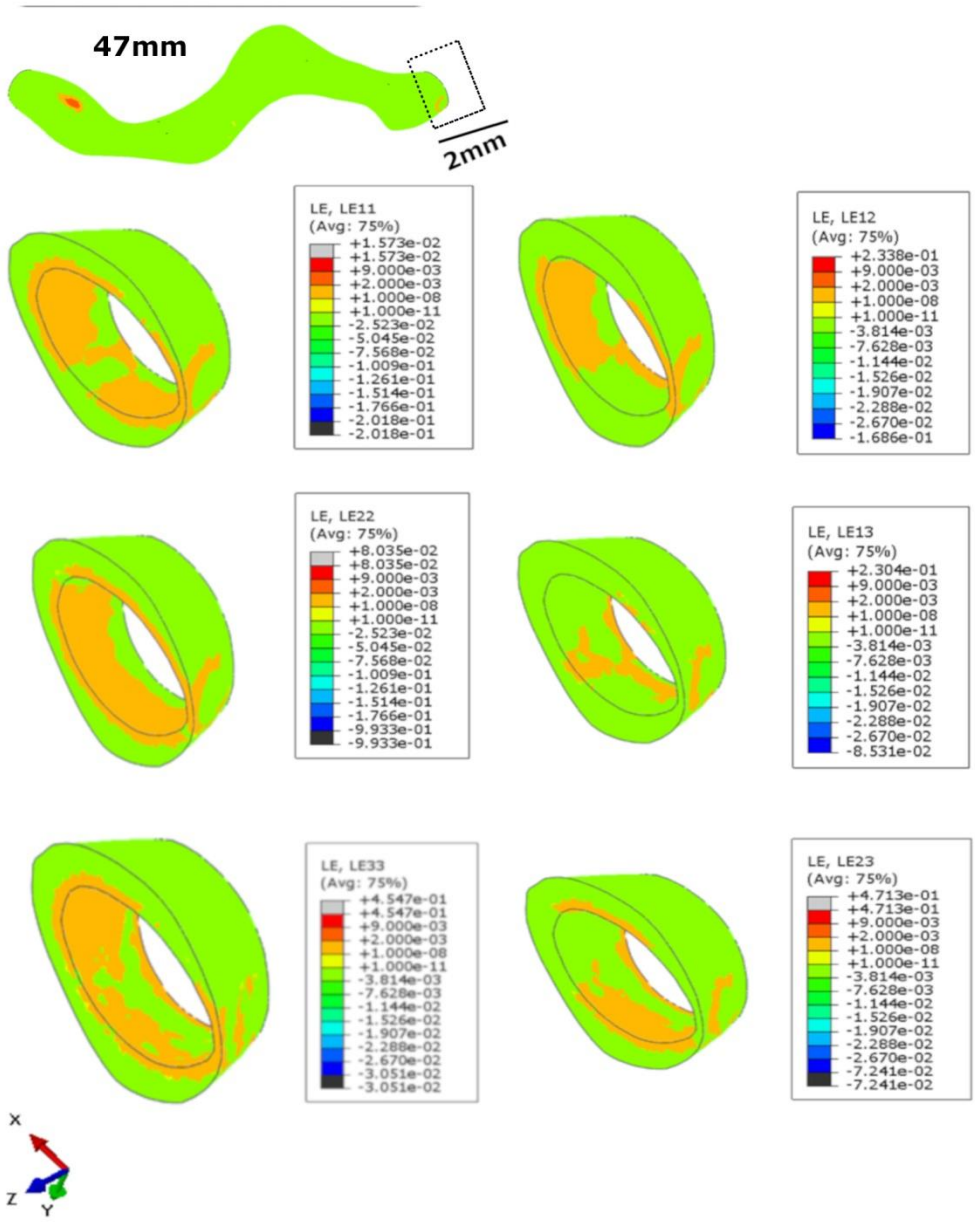

Figure 4.23: Logarithmic Strain rates on diseased model using FSI approach in six dimensions(11=xx,22=yy,zz=33,12=xy,13=xz,23=yz),showing maximum strain magnitude in yz dimension on a cut through from the outlet.

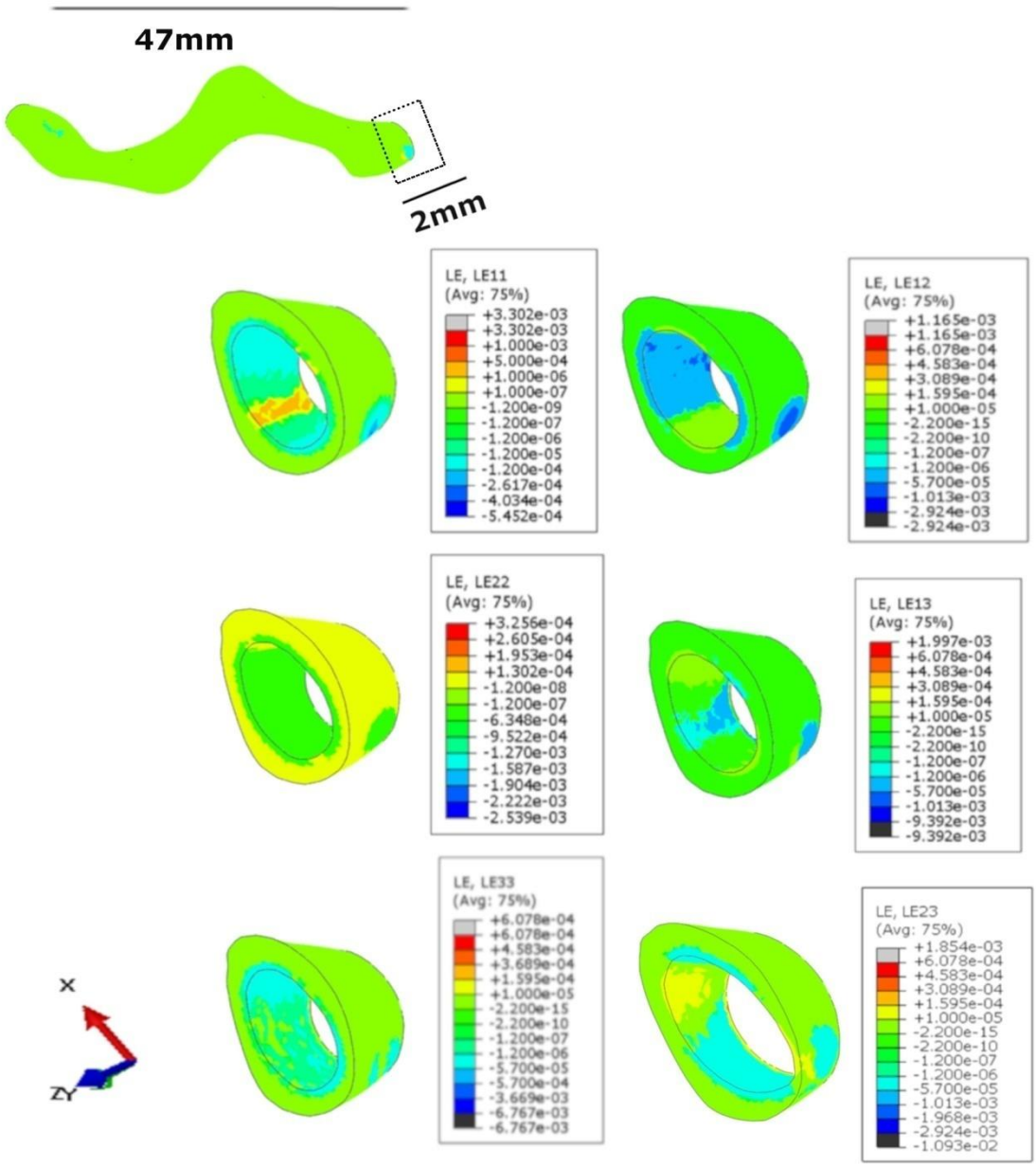

Figure 4.24: Logarithmic Strain rates on diseased model using Structure based approach in six dimensions(11=xx,22=yy,zz=33,12=xy,13=xz,23=yz),showing maximum strain magnitude in xx dimension on a cut through from the outlet.

4.2.4 Pressure Profile

Figure 4.25 is showing four healthy models of lumen from coarser to finer. Model with finite element size of 0.2mm shows the maximum pressure magnitude. The maximum pressure which the lumen (D) is imparting to the vessel wall is 2.967e+02 Pascal,and it is located at the intrados of bend where compressive forces have a significant role.

Whereas diseased lumen shows maximum pressure of 1.937e+08 Pascal (Figure 4.26) and it is located at the area where lumen is so much obstructed.

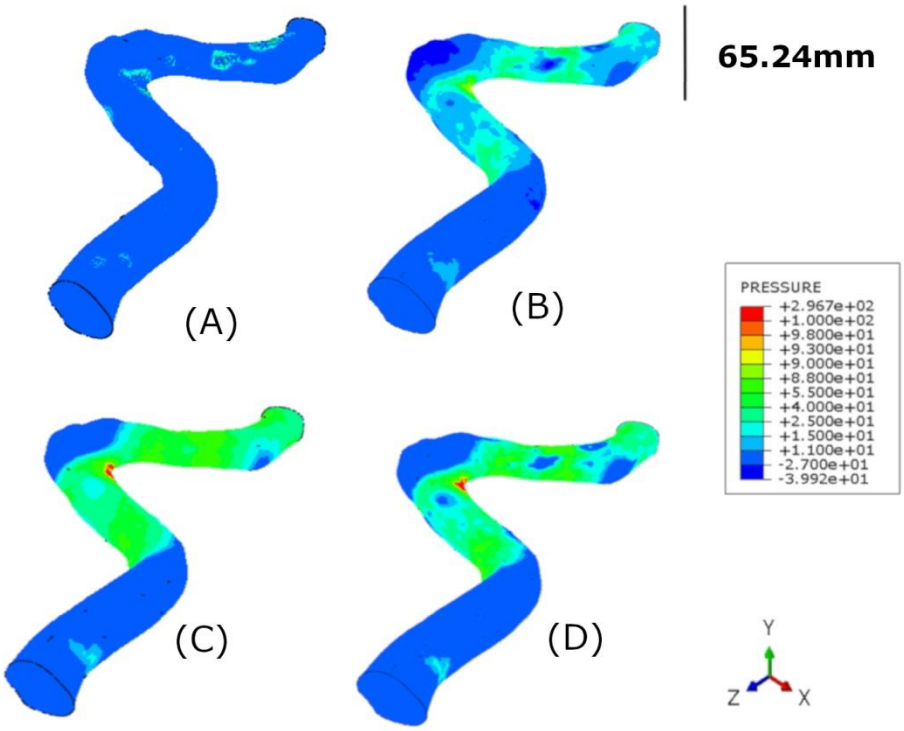

Figure 4.25: Pressure plots on Healthy lumen using FSI. (A) Model with finite element size of 0.5mm; (B) Model (edge length: 0.4mm); (C) Model (edge length:0.3mm); (D)Model (edge length:0.2mm) showing maximum pressure.

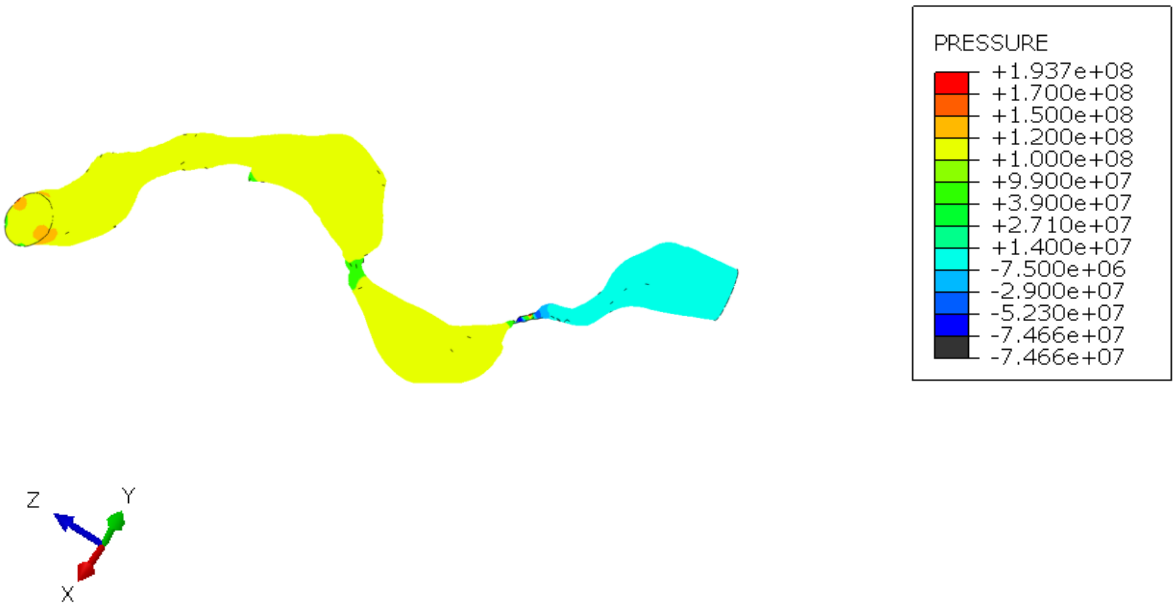

Figure 4.26: Pressure Distribution in Diseased Model showing maximum pressure at the highest occlusion.

4.3 Calcium Scoring Results

Calcium score found in our study is 105.3(volume 115.686 mm3) which correspond to the moderate level of disease. Script of Algorithm is attached in Appendix A.

4.4 Cardiovascular Analogy with Plumbing System

The cardiovascular circulatory system of the human body can be compared with a network of tubes. It consists of a pump and a system of branched vessels. Small diameter pipes are usually referred to as tubes. Usually, liquid fluids are transported in circular pipes. This is because pipes with a circular cross section can withstand large pressure differences between the inside and the outside without undergoing significant distortion (Cengel and Ghajar, 2011).

Let p1 and p2 be the points at the inlet and outlet (Figure 4.27-a). The pressure difference ΔP between two points along a tube originates a flow F directly proportion to Δp (Figure 4.27-a).To

elaborate this, if we consider a fluid entering a circular pipe at a uniform velocity. Because of the no-slip condition, the fluid particles in the layer in contact with the surface of the pipe come to a complete stop. This layer also causes the fluid particles in the adjacent layers to slow down gradually as a result of friction (Figure 4.27-b). To make up for this velocity reduction, the velocity of the fluid at the midsection of the pipe has to increase to keep the mass flow rate through the pipe constant. As a result, a velocity gradient develops along the pipe.

In cases where there is a three-dimensional flow field, the flow is often regarded as comprising two components, a primary flow and a secondary flow. The primary flow is parallel to the main direction of fluid motion and the secondary flow is perpendicular to this. At bends and bifurcations secondary flows usually occurs (Figure 4.28)(Malkin and Malkin, 1994).

To fully understand mechanics and dynamics of plumbing system, it is important to know what kind of forces act upon "fittings", bends and bifurcations of pipes. In bends, the centrifugal forces cause a radial pressure increase from the inner to the outer wall. Presence of this internal pressure has a considerable effect on load-deformation behavior. The applied force caused by water-pipe interaction induces deformation in pipe which is usually adjacent to bends. As a result increased curvature of the bend may cause buckling or fracture of pipe(Liepsch, 1986).

The visualization of the Von Mises stress distribution by Celal also confirms that internal pressure dramatically increases the von Mises stress and strain at the compression side of the wrinkle location(Cakiroglu et al., 2012).

High shear stresses are measured generally at the boundary between forward and reverse flow. These shear stresses are reduced by about 25% depending on the elasticity of the wall. In arteries forward and reverse flows are due to systolic and diastolic environment within heart(Liepsch, 1986).

There are some fundamental similarities between tube flow and arterial flow. Deformation and stress patterns shows good similarity whereas the flow pattern is quite different because of the pulsatility, elasticity of the wall and non-Newtonian flow behavior of blood. As far as plaque deposits are concerned, they can be correlated with the algal boom in dead water zones.

$$P1-P2= \Delta P$$

$$F \propto \Delta P$$

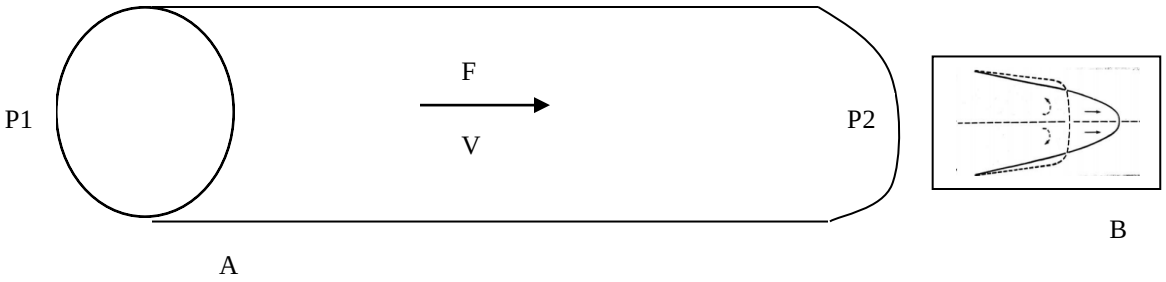

Figure 4.27: Flow origination within a pipe (A) and Velocity profile for a laminar flow (B) (Liepsch, 1986);

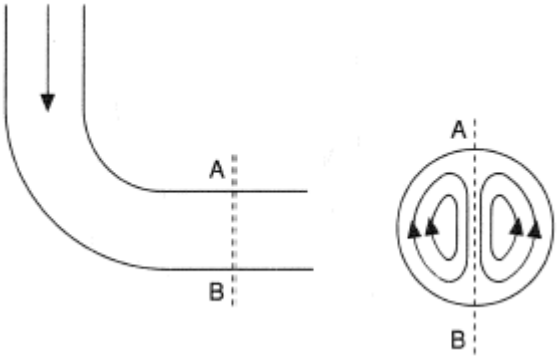

Figure 4.28:Pipe cross-section showing Secondary Flow at bent (Malkin and Malkin, 1994)

CHAPTER 5: Discussion

In this study modeling and simulation of atherosclerotic coronary artery is presented to quantify its mechanical strength .Mechanical environment of both healthy and diseased model is compared to highlight the characteristics of atherosclerosis. Individual of same age group and Gender are chosen to draw a significant conclusion. For 3D modeling and mesh creation Mimics, Materialize has utilized while Abaqus CAE is being used to measure 3d flow induced mechanical response of artery through finite element coupling. Results are validated and compared through DIC as well as with the past experimental and theoretical data from literature.

Five parameters are taken into account in this study named Deformation, Von Mises Stress, Shear Stress, Logarithmic Strain and Pressure.

In 2009 Ryo and coworkers performed a fully coupled FSI study to test out the effect of wall compliance on hemodynamics of coronary artery (Torii et al., 2009). Maximum deformation of vessel wall recorded by them was 3.85mm which is close to the value determined in this study (3.799mm).To date, both in vivo and in vitro studies has been carried out to find out displacement of coronary artery, however displacement values determined in vivo are large comparably to the simulation value(Torii et al., 2009, Pasterkamp et al., 2000, Ohayon et al., 2014).(Ding et al., 2002) conducted one such study and found maximum displacement as 60 mm. Previous literature indicates that atherosclerosis lead to increased stiffness of an artery(Cecelja and Chowienczyk, 2012, van Popele et al., 2001).This trend is clear in our results obtained from structural analysis(1.6mm to 0.0596mm).However results of diseased FSI analysis shows a slight increase in deformation(maximum) probably at the region where walls are thin.(Valencia and Villanueva, 2006) determined maximum deformation as 0.64mm which synchronizes with our results.

Zhi-Yong Li (2008) determined stress on vessel wall based on different lumen shapes(Li and Gillard, 2008). Stress scale ranges from 42420 Pa (circular lumen) to 242600 Pa (crescent lumen). In 2006 Alvaro and Martin performed simulation of blood flow in a 70% stenosed symmetric and non symmetric artery. Maximum wall stress predicted by them was 230000 Pa and 248000 Pa(Valencia and Villanueva, 2006).In our study Maximum Von Mises Stress predicted is 516.3 Pa (healthy vessel) which has increased to 94720 Pa in atherosclerotic model.

Our results are in exact correlation with a recent simulation study (Alishahi et al., 2011) which measured 91,390 Pa as maximum Von Mises stress.

Unsteady flow in stenotic arteries using FSI approach was studied(Alvaro A Valencia 2006) and wall shear stress was predicted at different stenotic levels(50% to 80%).Their predicted WSS range was 1553 Pa(at 50% stenosis) to 1726 Pa (at 80% stenosis)which is in accordance with our finding(1967 Pa).

In healthy model the predicted maximum luminal pressure in our study is 296.7 Pa whereas in diseased model it has increased upto 1.937e+08 Pa because of stenosis.(Saxena et al., 2016) published a CFD study of blood flow in human aorta and found 19430 Pa as maximum pressure.In another study (Moumen, 2016) 10820 Pa was computed as maximum pressure.(Kallekar et al., 2017) observed the maximum pressure as 574 Pa in a stenosed artery model. A study conducted in 2010 (by Joris Degroote) predicted 1400 Pa pressure in an FSI study of flexible tubes. In comparison with literature our diseased model is showing overestimated results probably due to the high complexity at stenosis region.

Our healthy model is exhibiting 0.004 and 0.006 as maximum logarithmic strain through both FSI and structural approaches respectively. Strain rates have decreased in diseased models. In 2002 chen yen ooi estimated local mechanical properties of atherosclerotic artery(Ooi et al., 2012). They developed Finite Element models of arterial rings to calculate logarithmic strain. Highest recorded strain value by them was 0.308. Mehmet H. Kural in 2012 observed 0 .08 and 0 .065 as maximum principal strain(Kural et al., 2012).

To conclude,Blood flow was simulated in an artery to analyze the mechanical behavior of vessel wall. Several parameters were studied to establish a link between hemodynamics and structural mechanics in arterial blood flow. Both normal and atherosclerotic model was assessed using both FSI and structural approach. Rupture risk of stage v models was predicted. Overall result of the study is in accordance with the previous findings.

CHAPTER 6: Conclusion and Future work

Below are the highlighted points of our study:

The problem of atherosclerotic cardiovascular disease (ACD) being the leading cause of mortality worldwide requires improved prognosis procedures.FSI because of its ability to give solution in both domains (structure and fluid) is a powerful and reliable method to investigate atherosclerosis.

- Atherosclerosis leads to decrease in deformation of vessel wall as compared to the healthy arterial model due to the overtime accumulation of plaque deposits in it hence lead to hardening of artery.

- In healthy model Von Mises stress is maximum at the intrados of bend which is under tortional loading making this site more vulnerable to plaque development.

- Diseased model is revealing more Von mises stress comparable to healthy model because of arterial occlusion.
- WSS is greater in unhealthy case because cross sectional area of lumen is reduced, which increases velocity and produces larger WSS.It could be the reason why stenosed region is more prone to complete obstruction.

- Strain rates predicted using structure based analysis are high in healthy arteries as compared to the diseased atherosclerotic arteries. However, as datasets belongs to two different individuals, difference of vessel shape and its associated mechanical environment could be the reason of low strain rates in healthy models using FSI.

- Calcified plaque probably due to its location and geometry is more unstable while fibrous plaque is exhibiting the stiffest response to loading. This is very similar to one of the

studies in literature (Schmermund and Erbel, 2001) demonstrating calcified plaque as a marker for the unstable process.

- Calcium Score of 105.3 is contributing to overall plaque burden categorizing a stage v atherosclerotic artery on moderate risk.

Limitations of study are as under:

- Vessel wall is composed of three layers named intima media and adventitia (from inside to outside) whereas in this study combined thickness of all three layers is given to a single vessel layer. Further study could be carried out to investigate the stress-strain response of individual layer.
- Cardiac cycle has two phases called systolic and diastolic due to which blood flows in a pulsatile fashion in heart.Pulsatility is not considered in this study and a homogenous velocity in provided at the inlet which I think in future could be addressed.
- In some previous studies different imaging modalities have been used to confirm and validate the results of segmentation (particular plaque).However this study is based on just CT modality.
- Material properties of vessel wall and plaque are taken from the literature however mechanical testing on cadaver arteries could give more accurate results.
- In future different blood flow models including non Newtonian model can be examined.
- Finally, the current study is only performing risk stratification of stage v model. However to study the progression and development of atherosclerosis follow up visits of same patient should be monitored.

APPENDIX A

Script

```
defcomputeAgatstonScore(volumeNode, verbose=False):
importnumpy as np
import math
voxelArray = slicer.util.arrayFromVolume(volumeNode)
  areaOfPixelMm2       =       volumeNode.GetSpacing()[0]       *
volumeNode.GetSpacing()[1]
numberOfSlices = voxelArray.shape[0]
totalScore = 0
forsliceIndex in range(numberOfSlices):
voxelArraySlice = voxelArray[sliceIndex]
maxIntensity = voxelArraySlice.max()
ifmaxIntensity< 100:
continue
weightFactor = math.floor(maxIntensity/100)
indicesOfNonZeroVoxels = np.where(voxelArraySlice>100)
numberOfNonZeroVoxels = len(indicesOfNonZeroVoxels[0])
sliceScore    =    numberOfNonZeroVoxels    *    areaOfPixelMm2    *
weightFactor
totalScore += sliceScore
if verbose:
print("Slice score: {1}".format(sliceIndex, sliceScore))
slicer.app.processEvents()
returntotalScore

print("Total                    Agatston                    score:
{0}".format(computeAgatstonScore(getNode('2:    web    CS,    78.0%
masked'))))
Total Agatston score: 105.303
```

REFERENCES

The progression of atherosclerosis

[Online]. Available: https://en.wikipedia.org/wiki/Atherosclerosis.

OCT 22 2012. *UNDERSTANDING THE THREE MAIN STAGES OF PLAQUE GROWTH* [Online]. Available: https://preventivecardiologist.wordpress.com/2012/10/22/understanding-the-three-main-stages-of-plaque/ [Accessed 9/3/2018 2018].

ALISHAHI, M., ALISHAHI, M. & EMDAD, H. 2011. Numerical simulation of blood flow in a flexible stenosed abdominal real aorta. *Scientia Iranica,* 18**,** 1297-1305.

ATABEK, H. & LEW, H. 1966. Wave propagation through a viscous incompressible fluid contained in an initially stressed elastic tube. *Biophysical Journal,* 6**,** 481.

BEULEN, B., RUTTEN, M. & VAN DE VOSSE, F. 2009. A time-periodic approach for fluid-structure interaction in distensible vessels. *Journal of Fluids and Structures,* 25**,** 954-966.

BRATER, E. F., KING, H. W., LINDELL, J. E. & WEI, C. 1976. *Handbook of hydraulics for the solution of hydraulic engineering problems,* McGraw-Hill New York.

BUDOFF, M. J., HOKANSON, J. E., NASIR, K., SHAW, L. J., KINNEY, G. L., CHOW, D., DEMOSS, D., NUGURI, V., NABAVI, V. & RATAKONDA, R. 2010. Progression of coronary artery calcium predicts all-cause mortality. *JACC: Cardiovascular Imaging,* 3**,** 1229-1236.

BUDOFF, M. J., YOUNG, R., LOPEZ, V. A., KRONMAL, R. A., NASIR, K., BLUMENTHAL, R. S., DETRANO, R. C., BILD, D. E., GUERCI, A. D. & LIU, K. 2013. Progression of coronary calcium and incident coronary heart disease events: MESA (Multi-Ethnic Study of Atherosclerosis). *Journal of the American College of Cardiology,* 61**,** 1231-1239.

CAKIROGLU, C., KOMEILI, A., ADEEB, S., CHENG, J. R. & SEN, M. Numerical analysis of high pressure cold bend pipe to investigate the behaviour of tension side fracture. 2012 9th International Pipeline Conference, 2012. American Society of Mechanical Engineers, 273-278.

CECELJA, M. & CHOWIENCZYK, P. 2012. Role of arterial stiffness in cardiovascular disease. *JRSM cardiovascular disease,* 1**,** 1-10.

CENGEL, Y. A. & GHAJAR, A. 2011. Heat and mass transfer (a practical approach, SI version). McGraw-Hill Education.

CHATTERJEE, T. K., STOLL, L. L., DENNING, G. M., HARRELSON, A., BLOMKALNS, A. L., IDELMAN, G., ROTHENBERG, F. G., NELTNER, B., ROMIG-MARTIN, S. A. & DICKSON, E. W. 2009. Proinflammatory phenotype of perivascular adipocytes: influence of high-fat feeding. *Circulation research,* 104**,** 541-549.

CONTRIBUTORS, W. 2012. *Human Physiology*, Blacksleet River.

CONTROL, C. F. D. & PREVENTION Data are from the Multiple Cause of Death Files, 1999–2013, as compiled from data provided by the 57 vital statistics jurisdictions through the Vital Statistics Cooperative Program: National Center for Health Statistics. Underlying Cause of Death 1999–2013 on CDC WONDER Online Database, released 2015, 2015.

COSTOPOULOS, C., HUANG, Y., BROWN, A. J., CALVERT, P. A., HOOLE, S. P., WEST, N. E., GILLARD, J. H., TENG, Z. & BENNETT, M. R. 2017. Plaque rupture in coronary atherosclerosis is associated with increased plaque structural stress. *JACC: Cardiovascular Imaging***,** 2317.

DAWN 2017. More Pakistanis at risk from heart disease.

DE KREUTZENBERG, S. V., FADINI, G. P., GUZZINATI, S., MAZZUCATO, M., VOLPI, A., CORACINA, A. & AVOGARO, A. 2015. Carotid plaque calcification predicts future cardiovascular events in type 2 diabetes. *Diabetes Care***,** dc150327.

DEBAKEY, M. E., LAWRIE, G. M. & GLAESER, D. H. 1985. Patterns of atherosclerosis and their surgical significance. *Annals of surgery,* 201**,** 115.

DEGROOTE, J. 2010. *Development of algorithms for the partitioned simulation of strongly coupled fluid-structure interaction problems.* Ghent University.

DHAWAN, S. S., AVATI NANJUNDAPPA, R. P., BRANCH, J. R., TAYLOR, W. R., QUYYUMI, A. A., JO, H., MCDANIEL, M. C., SUO, J., GIDDENS, D. & SAMADY, H. 2010. Shear stress and plaque development. *Expert review of cardiovascular therapy,* 8**,** 545-556.

DING, Z., ZHU, H. & FRIEDMAN, M. H. 2002. Coronary artery dynamics in vivo. *Annals of biomedical engineering,* 30**,** 419-429.

GILMAN, J. J. 1969. *Micromechanics of flow in solids*, McGraw-Hill.

GOUBERGRITS, L., WELLNHOFER, E. & KERTZSCHER, U. Choice and Impact of a Non-Newtonian Blood Model for Wall Shear Stress Profiling of Coronary Arteries. 14th Nordic-Baltic Conference on Biomedical Engineering and Medical Physics, 2008. Springer, 111-114.

HAN, H.-C., CHESNUTT, J. K., GARCIA, J. R., LIU, Q. & WEN, Q. 2013. Artery buckling: new phenotypes, models, and applications. *Annals of biomedical engineering,* 41**,** 1399-1410.

JOHNSTON, B. M., JOHNSTON, P. R., CORNEY, S. & KILPATRICK, D. 2004. Non-Newtonian blood flow in human right coronary arteries: steady state simulations. *Journal of biomechanics,* 37**,** 709-720.

KALLEKAR, L., VISWANATH, C. & ANAND, M. 2017. Effect of Wall Flexibility on the Deformation during Flow in a Stenosed Coronary Artery. *Fluids,* 2**,** 16.

KLAINERMAN, S. & MAJDA, A. 1982. Compressible and incompressible fluids. *Communications on Pure and Applied Mathematics,* 35**,** 629-651.

KURAL, M. H., CAI, M., TANG, D., GWYTHER, T., ZHENG, J. & BILLIAR, K. L. 2012. Planar biaxial characterization of diseased human coronary and carotid arteries for computational modeling. *Journal of biomechanics,* 45**,** 790-798.

KWAK, B. R., BÄCK, M., BOCHATON-PIALLAT, M.-L., CALIGIURI, G., DAEMEN, M. J., DAVIES, P. F., HOEFER, I. E., HOLVOET, P., JO, H. & KRAMS, R. 2014. Biomechanical factors in atherosclerosis: mechanisms and clinical implications. *European heart journal,* 35**,** 3013-3020.

LEACH, J. R., RAYZ, V. L., MOFRAD, M. R. & SALONER, D. 2010. An efficient two-stage approach for image-based FSI analysis of atherosclerotic arteries. *Biomechanics and modeling in mechanobiology,* 9**,** 213-223.

LI, Z.-Y. & GILLARD, J. H. 2008. Plaque rupture: plaque stress, shear stress, and pressure drop. *Journal of the American College of Cardiology,* 52**,** 499-500.

LIEPSCH, D. 1986. Flow in tubes and arteries-a comparison. *Biorheology,* 23**,** 395-433.

MALKIN, A. & MALKIN, A. Y. 1994. *Rheology fundamentals,* ChemTec Publishing.

MOINI, J. 2013. *Phlebotomy: Principles and Practice,* Jones & Bartlett Learning.

MOUMEN, F. 2016. Computational Fluid Dynamics Analysis of the Aortic Coarctation. *Natural Science,* 8**,** 271.

NAGY, E. 2010. The Effect of Calcified Plaque on Stress within a Fibrous Thin Cap Atheroma in an Atherosclerotic Coronary Artery Using Finite Element Analysis (FEA).

OHAYON, J., FINET, G., LE FLOC'H, S., CLOUTIER, G., GHARIB, A. M., HEROUX, J. & PETTIGREW, R. I. 2014. Biomechanics of atherosclerotic coronary plaque: site, stability and in vivo elasticity modeling. *Annals of biomedical engineering,* 42**,** 269-279.

OOI, C. Y., SUTCLIFFE, M. & DAVENPORT, A. 2012. A NOVEL APPROACH FOR ESTIMATING THE LOCAL MECHANICAL PROPERTIES OF ATHEROSCLEROTIC ARTERY. *Journal of Biomechanics,* 45**,** S10.

OSCUII, H. N., SHADPOUR, M. T. & GHALICHI, F. 2007. Flow characteristics in elastic arteries using a fluid-structure interaction model. *American Journal of Applied Sciences,* 4**,** 516-524.

PASTERKAMP, G., FALK, E., WOUTMAN, H. & BORST, C. 2000. Techniques characterizing the coronary atherosclerotic plaque: influence on clinical decision making? *Journal of the American College of Cardiology,* 36**,** 13-21.

S ANTONOPOULOS, A., MARGARITIS, M., LEE, R., CHANNON, K. & ANTONIADES, C. 2012. Statins as anti-inflammatory agents in atherogenesis: molecular mechanisms and lessons from the recent clinical trials. *Current pharmaceutical design,* 18**,** 1519-1530.

SAXENA, Y., GUPTA, R., MOINUDDIN, A. & NARWAL, R. 2016. Blood pressure reduction following accumulated physical activity in prehypertensive. *Journal of family medicine and primary care,* 5**,** 349.

SCHMERMUND, A. & ERBEL, R. 2001. Unstable coronary plaque and its relation to coronary calcium. *Circulation,* 104**,** 1682-1687.

SCHROEDER, S., KOPP, A. F., BAUMBACH, A., MEISNER, C., KUETTNER, A., GEORG, C., OHNESORGE, B., HERDEG, C., CLAUSSEN, C. D. & KARSCH, K. R. 2001. Noninvasive detection and evaluation of atherosclerotic coronary plaques with multislice computed tomography. *Journal of the American College of Cardiology,* 37**,** 1430-1435.

SYSTEMES, D. 2010. Introduction to Abaqus/CFD. *Dassualt Systemes***,** 1-218.

TANG, D., YANG, C., ZHENG, J., WOODARD, P. K., SICARD, G. A., SAFFITZ, J. E. & YUAN, C. 2004. 3D MRI-based multicomponent FSI models for atherosclerotic plaques. *Annals of biomedical engineering,* 32**,** 947-960.

TORII, R., WOOD, N. B., HADJILOIZOU, N., DOWSEY, A. W., WRIGHT, A. R., HUGHES, A. D., DAVIES, J., FRANCIS, D. P., MAYET, J. & YANG, G. Z. 2009. Fluid–structure interaction analysis of a patient-specific right coronary artery with physiological velocity and pressure waveforms. *Communications in numerical methods in engineering,* 25**,** 565-580.

VALENCIA, A. & VILLANUEVA, M. 2006. Unsteady flow and mass transfer in models of stenotic arteries considering fluid-structure interaction. *International Communications in Heat and Mass Transfer,* 33**,** 966-975.

VAN POPELE, N. M., GROBBEE, D. E., BOTS, M. L., ASMAR, R., TOPOUCHIAN, J., RENEMAN, R. S., HOEKS, A. P., VAN DER KUIP, D. A., HOFMAN, A. & WITTEMAN, J. C. 2001. Association between arterial stiffness and atherosclerosis: the Rotterdam Study. *Stroke,* 32**,** 454-460.

VOGEL, R. A. 1997. Coronary risk factors, endothelial function, and atherosclerosis: a review. *Clinical cardiology,* 20**,** 426-432.

WARBOYS, C. M., AMINI, N., DE LUCA, A. & EVANS, P. C. 2011. The role of blood flow in determining the sites of atherosclerotic plaques. *F1000 medicine reports,* 3.

WASILEWSKI, J., NIEDZIELA, J., OSADNIK, T., DUSZAŃSKA, A., SRAGA, W., DESPERAK, P., MYGA-POROSIŁO, J., JACKOWSKA, Z., NOWAKOWSKI, A. & GŁOWACKI, J. 2015. Predominant location of coronary artery atherosclerosis in the left anterior descending artery. The impact of septal perforators and the myocardial bridging effect. *Kardiochirurgia i torakochirurgia polska= Polish journal of cardio-thoracic surgery,* 12**,** 379.